

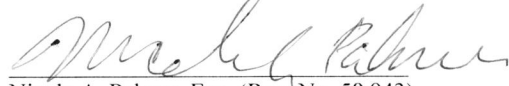
Attorney Docket No. S2007-2013  
Mark: PARYLENE HT  
Examiner: Ramona Ortiga Palmer  
U.S. Serial No.: 76/711,510

**IN THE UNITED STATES PATENT AND TRADEMARK OFFICE**

Applicant: Specialty Coating Systems, Inc.  
Serial No.: 76/711,510  
Filing Date: May 16, 2012  
Mark: PARYLENE HT  
Int'l Class Nos.: 002 & 040  
Examiner: Ramona Ortiga Palmer  
Law Office: 117

**CERTIFICATE OF MAILING UNDER 37 C.F.R. § 2.197**

The undersigned hereby certifies that this document and enclosures are being placed in the United States mail with first-class postage attached, addressed to the Commissioner for Trademarks, P.O. Box 1451, Alexandria, VA 22313-1451 on August 24, 2015.

  
Nicole A. Palmer, Esq. (Reg. No. 58,943)

Commissioner for Trademarks  
P.O. Box 1451  
Alexandria, VA 22313-1451

**TRANSMITTAL**

Sir:

Transmitted herewith are the following documents in connection with the above-identified trademark application:

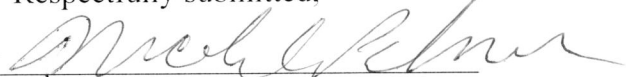
- Response to a Final Office Action mailed February 23, 2015 (2 pgs.)
- Supplemental Declaration Under Section 2(f) Pursuant to 15 U.S.C. § 1052(f) (2 pgs.)
- Exhibits A-C (10 pgs.)
- Notice of Appeal
- Return Postcard

If the enclosed papers are considered incomplete, the Mail Room and/or the Application Branch are respectfully requested to contact the undersigned at (617) 395-7000, Cambridge, Massachusetts.

The Commissioner is hereby authorized to charge the Appeal Fee along with any other deficiency or overpayment to Deposit Account No. 50/2762, Ref. No. S2007-2013. A duplicate copy of this transmittal is enclosed.

Respectfully submitted,

By:



Nicole A. Palmer, Esq. (Reg. No. 58,943)  
LANDO & ANASTASI, LLP  
Riverfront Office Park  
One Main Street  
Cambridge, MA 02142  
Tel.: (617) 395-7000; Fax: (617) 395-7070  
Attorney for Applicant



08-27-2015

U.S. Patent & TMO/ TM Mail Rpt Dt. #22

Dated: August 24, 2015  
Attorney Docket No.: S2007-2013

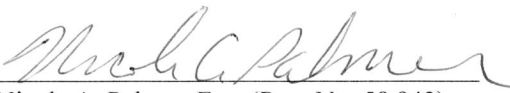
**IN THE UNITED STATES PATENT AND TRADEMARK OFFICE  
BEFORE THE TRADEMARK TRIAL AND APPEAL BOARD**

Applicant: Specialty Coating Systems, Inc.  
 Serial No.: 76/711,510  
 Filing Date: May 16, 2012  
 Mark: PARYLENE HT  
 Int'l Class Nos.: 002 & 040  
 Examiner: Ramona Ortiga Palmer  
 Law Office: 117

Certificate of First-Class Mailing

I hereby certify that the enclosed materials are being deposited with the United States Postal Service as first class mail under 37 CFR 2.197 in an envelope addressed to Commissioner for Trademarks, P.O. Box 1451, Alexandria, Virginia 22313-1451 on the date set forth below.

August 24, 2015  
 \_\_\_\_\_  
 (Date)

  
 \_\_\_\_\_  
 Nicole A. Palmer, Esq. (Reg. No. 58,943)

Trademark Trial and Appeal Board  
 Commissioner for Trademarks  
 P.O. Box 1451  
 Alexandria, VA 22313-1451

**NOTICE OF APPEAL AND REQUEST FOR RECONSIDERATION**

Applicant hereby appeals to the Trademark Trial and Appeal Board from the decision of the Examining Attorney dated February 23, 2015, refusing registration of Applicant's trademark. This is a precautionary Notice of Appeal. Applicant files concurrently herewith a timely Response to Final Office Action, and Applicant requests reconsideration of the rejection in light of that submission. This precautionary Notice is being filed to avoid inadvertent abandonment.

08/28/2015 DJEFFCOA 00000002 502762 76711510  
 01 FC:6403 100.00 DA

Respectfully submitted,

  
 \_\_\_\_\_  
 Nicole A. Palmer, Esq. (Reg. No. 58,943)  
 LANDO & ANASTASI, LLP  
 Riverfront Office Park  
 One Main Street; Eleventh Floor  
 Cambridge, MA 02142  
 Tel.: (617) 395-7000; Fax: (617) 395-7070  
 Attorney for Applicant

Date: August 24, 2015  
 Attorney Docket No.: S2007-2013

**IN THE UNITED STATES PATENT AND TRADEMARK OFFICE**

Applicant: Specialty Coating Systems, Inc.  
Serial No.: 76/711,510  
Filing Date: May 16, 2012  
Mark: PARYLENE HT  
Int'l Class Nos.: 002 and 040  
Examiner: R. O. Palmer  
Law Office: 117

---

**CERTIFICATE OF MAILING UNDER 37 C.F.R. § 2.197**

The undersigned hereby certifies that this document and any noted enclosures are being placed in the United States mail with first-class postage attached, addressed to the Commissioner for Trademarks, P.O. Box 1451, Alexandria, VA 22313-1451 on August 24, 2015.

  
Nicole A. Palmer, Esq. (Reg. No. 58,943)

---

Commissioner for Trademarks  
P.O. Box 1451  
Alexandria, VA 22313-1451

**REQUEST FOR RECONSIDERATION IN RESPONSE TO FINAL OFFICE ACTION**

This paper is submitted in response to the Final Office Action that was mailed on February 23, 2015. Applicant herein submits additional remarks in support of registration. A precautionary Notice of Appeal is submitted herewith.

**REMARKS**

**I. Acquired Distinctiveness**

The Final Office Action maintained the rejection of the registration under Trademark Act Section 2(e)(1) and indicated that additional evidence is needed.

Applicant previously amended the application to assert acquired distinctiveness based on more than five years' use in commerce. A supplemental Declaration under Trademark Act Section 2(f) pursuant to 35 U.S.C. Section 1052(f) was submitted on September 17, 2013 to provide additional evidence in support of Applicant's claim of acquired distinctiveness. Further

Applicant: Specialty Coating Systems, Inc.  
U.S.S.N.: 76/711,510

comments in support of registration were presented in the Response to Office Action submitted on January 22, 2015.

The previously submitted evidence including samples of advertising and consumer statements of recognition should be considered supportive of Applicant's acquired distinctiveness claim along with the length and exclusivity of related use.

A further Supplemental Declaration under Trademark Act Section 2(f) pursuant to 35 U.S.C. Section 1052(f) accompanies this submission to provide additional evidence in support of Applicant's claim of acquired distinctiveness. Specifically, the supplemental Declaration by Applicant provides relevant information regarding marketing and sales, along with additional examples of industry recognition attributing the mark to Applicant.

The proposed mark is not merely descriptive and the Section 2(e)(1) ground for rejection is believed to be obviated.

With particular reference to International Class 040, Applicant respectfully disagrees that the proposed mark is merely descriptive in view of the relevant identification of goods/services which makes no reference to coating with a polymer material, let alone with a parylene material.

Reconsideration is respectfully requested in view thereof.

## **II. Conclusion**

In view of this response, the application is believed to be in condition for allowance. Prompt passage to publication is therefore in order and requested.

Any questions regarding this submission may be directed to Applicant's representative at the telephone number provided below.

Respectfully Submitted,



Nicole A. Palmer, Esq. (Reg. No. 58,943)

LANDO & ANASTASI, LLP

Riverfront Office Park

One Main Street; Eleventh Floor

Cambridge, MA 02142

Tel.: (617) 395-7000

Attorney for Applicant

Dated: August 24, 2015

Attorney Docket No.: S2007-2013

**IN THE UNITED STATES PATENT AND TRADEMARK OFFICE**

Applicant: Specialty Coating Systems, Inc.  
Serial No.: 76/711,510  
Filing Date: May 16, 2012  
Mark: PARYLENE HT  
Int'l Class Nos.: 002 and 040  
Examiner: R. O. Palmer  
Law Office: 117

---

**CERTIFICATE OF MAILING UNDER 37 C.F.R. § 2.197**

The undersigned hereby certifies that this document and enclosures are being placed in the United States mail with first-class postage attached, addressed to the Commissioner for Trademarks, P.O. Box 1451, Alexandria, VA 22313-1451 on August 24, 2015.

  
Nicole A. Palmer, Esq. (Reg. No. 58,943)

---

Commissioner for Trademarks  
P.O. Box 1451  
Alexandria, VA 22313-1451

**Supplemental Declaration Under Section 2(f) Pursuant to 15 U.S.C. Section 1052(f)**

This paper supplements the Declaration previously submitted on September 17, 2013.

I, the undersigned, declare as follows:

The mark PARYLENE HT has become distinctive through Applicant's substantially exclusive and continuous use in commerce for at least the five years immediately preceding the filing date of the present trademark application.

Applicant has made, and continues to make, significant efforts in the United States to associate the mark PARYLENE HT with itself as a source identifier. Applicant routinely mentions the mark PARYLENE HT in a majority of its marketing materials. In terms of advertising figures, more than one-third of Applicant's total expenditure on marketing collateral over the relevant period has been at least partially directed to establishing brand awareness under

Applicant: Specialty Coating Systems, Inc.  
U.S.S.N.: 76/711,510

the mark PARYLENE HT. Examples of such advertisements referencing the mark PARYLENE HT were previously submitted.

In terms of sales volume, at least about 15% to about 20% of Applicant's production line sample runs over the relevant period have been attributable to the goods and services offered under the mark PARYLENE HT.

Unsolicited media coverage confirming that the purchasing public has come to view the mark PARYLENE HT as an indicator of origin was previously submitted.

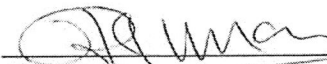
Additional examples of industry recognition are submitted herewith as Exhibits A-C in the form of journal articles referencing Applicant as the sole supplier of the relevant materials and exclusive coater of the evaluated samples under the mark PARYLENE HT.

The mark PARYLENE HT has therefore acquired distinctiveness and is not merely descriptive of the relevant goods and/or services.

The undersigned being warned that willful false statements and the like are punishable by fine or imprisonment, or both, under 18 U.S.C. § 1001, and that such willful false statements and the like may jeopardize the validity of the application or document or any registration resulting therefrom, declares that all statements made of his own knowledge are true; and all statements made on information and belief are believed to be true.

**Specialty Coating Systems, Inc., Applicant**

Date: 8/24/15

By:   
Name: Rakesh Kumar  
Title: Vice President, Technology

# Electrical Conduction in Parylene HT

S. Diaham, M.-L. Locatelli, R. Khazaka, H. Hourdequin

Université de Toulouse; UPS, INPT; LAPLACE (Laboratoire Plasma et Conversion d'Energie);  
118 Route de Narbonne, F-31062 Toulouse cedex 9, France.  
CNRS; LAPLACE; F-31062 Toulouse, France.

and R. Kumar

Specialty Coating Systems, Inc. (SCS); Cookson Electronics;  
7645 Woodland Drive, Indianapolis, IN 46278, USA.

## ABSTRACT

The electrical conduction of parylene HT films, a new high performance fluorinated parylene, is investigated at high temperature (200 to 350 °C), high electric field (50 and 3600 kV/cm) and for different thicknesses (1.2 to 11 μm). The steady-state currents are analysed by assuming different conduction models. Whereas the Schottky and Poole-Frenkel models have been excluded, the thermally assisted hopping mechanism appears as the most probable conduction mechanism for fields up to the threshold (~1500 kV/cm). Based on the analysis of the hopping jump distance and its evolution versus temperature, an ionic hopping conduction has been proposed as the most probable charge carriers origin to describe our results. Finally, the film thickness and the field polarity are studied. Results indicate that positive carriers (holes) are the main contributors to the injection current.

Index Terms — Parylene HT, Parylene-AF4, Poly(*α,α,α',α'*-tetrafluoro-*p*-xylylene), Electrical conduction, High temperature, Hopping conduction.

## 1 INTRODUCTION

POLYMERIC materials are widely used in the field of microelectronics where low dielectric constant materials with high electrical insulating performances are required as interlayer dielectrics (ILD) in the high-density multi-level interconnection to reduce the RC (resistance-capacitance) delay [1,2] or as passivation layer at the semiconductor surface [3]. Dielectric layers able to insure the insulation at high temperatures become of main interest due to the development of new wide band gap semiconductor devices and specially those founded on the most mature silicon carbide (SiC) technology able to operate at high temperature (200 °C - 400 °C). Polyparaxylylene (PPX) films, usually referred as parylenes (PA), appear as potential candidates for the surface electrical insulation of power electronic components due to their physical properties and the compatibility of their deposition process. The most prominent advantage is the solvent-less room temperature vapor deposition polymerization (VDP) process, allowing the deposition of conformal submicron and micron films (from 100 nm to 50 μm) without

forming pinholes [4,5]. Among all the kinds of parylene, fluorinated ones appear as the most adapted for high temperature applications. One of the most efficient fluorinated parylenes are from the family of Parylene AF4 and commercially available as Parylene HT (PA-HT). PA-HT owns a high thermal stability and good dielectric properties, making it potential candidates for the high temperature applications. In previous papers, some of the authors have investigated the evolution of the DC conductivity, the dielectric properties and the dielectric strength of PA-HT [6-8]. However, the electrical conduction mechanisms have not been reported yet and are of real interest since intermediate field levels correspond to real service conditions. In this paper, the conduction currents in PA-HT films are investigated at high temperatures from 200 °C to 350 °C well above the material glass transition temperature estimated in the range of 20 °C and 100 °C. The measurements using the current-time (*I-t*) methods were carried out for different electrical fields from 50 kV/cm up to 3.6 MV/cm. The effect of the film thickness and the applied voltage polarity on the conduction current will be investigated as well as the conduction mechanisms.

## 2 EXPERIMENTAL

### 2.1 MATERIAL AND TEST STRUCTURE

The electrical conduction properties were studied on 1.2  $\mu\text{m}$ , 4.9  $\mu\text{m}$  and 11  $\mu\text{m}$ -thick poly[(2,3,5,6-tetrafluoro-1,4-phenylene)(1,1,2,2-tetrafluoro-1,2-ethanediyl)] films, commercially available as Parylene HT<sup>®</sup> (Specialty Coating Systems, Inc. (SCS)) [9]. Figure 1 shows the monomeric structure of PA-HT. The films have been coated at room temperature onto mirror-polished stainless steel substrates (3.3 $\times$ 3.3  $\text{cm}^2$ ) by VDP using the Gorham process. Before the coatings, the substrates were cleaned with acetone and treated using an adhesion promoter (AdPro Plus<sup>®</sup>, SCS). Thicknesses were accurately measured (several times at different positions of each coating) with a KLA Tencor Alpha-A mechanical profilometer (accuracy in z-direction  $\pm 0.01 \mu\text{m}$ ). In order to avoid any structural variation in the films during the high temperature measurements, as highlighted previously [6,7], the films were annealed preliminary at 400  $^\circ\text{C}$  for 1 hour under nitrogen flux.

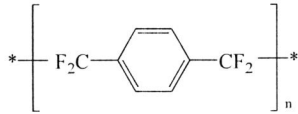


Figure 1. Chemical structure of the PA-HT (AF4 family) monomeric unit.

For the electrical characterizations, metal-insulator-metal (MIM) capacitance structures were achieved. Gold top electrodes (thickness of 180 nm) were evaporated under vacuum. Their geometrical shape and diameter were obtained by chemical etching of gold through a photo-resist mask owning circular patterns of 2 mm in diameter (see Figure 2).

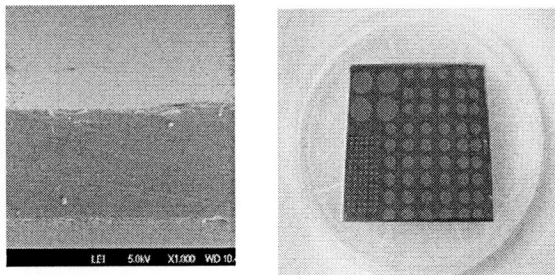


Figure 2. SEM image of the cross section of the PA-HT film (a) and top view of the MIM capacitor structures (b).

### 2.2 MEASUREMENT

The transient currents ( $I-t$ ) were measured for different applied electric fields using an electrometer Keithley 6517A allowing a voltage variation between 0 and 1000 V and the simultaneous measurement of the leakage current down to  $10^{-13}$  A (in our experimental conditions). The probe station was housed in a metal box (Faraday cage) which, in addition to the measurement noise reduction, protects the sample from room light during measurements to prevent possible photoelectric conduction. The voltage was applied

on the MIM structures connected to a needle-probe station. The positive polarity is applied on the top gold electrode unless otherwise stated. For high temperature measurements, the samples were placed on a thermally-regulated chuck with an accuracy of  $\pm 1 \text{ }^\circ\text{C}$  checked with a thermocouple on the sample surface. The samples were heated at a rising rate of 5  $^\circ\text{C}/\text{min}$  up to setting temperature (i.e. 200  $^\circ\text{C}$ , 250  $^\circ\text{C}$ , 300  $^\circ\text{C}$  or 350  $^\circ\text{C}$ ). They were thermalized during 5 minutes before measurements. Virgin samples were used for each tested temperature in order to avoid thermal history in PA-HT films. Once the field is applied, the transient current has been measured during more than 200 seconds. For each measurement, an untested electrode was used to avoid electrical history and all experiments were continued for long enough time periods to reach a relatively constant current value.

## 3 RESULTS AND DISCUSSION

### 3.1 TRANSIENT CURRENTS

Figure 3 shows the transient current density versus time between 200  $^\circ\text{C}$  and 350  $^\circ\text{C}$  for different applied electric fields for the 1.2- $\mu\text{m}$  PA-HT thick films. Consecutively to the application of the field, the current density shows a continuous decrease with time until reaching a time-independent value more or less quickly depending on temperature. Moreover, a global increase of the current magnitudes with increasing temperature indicates a thermal activation of the conduction mechanisms.

Usually, the current decay versus time in dielectrics obeys to the law of Curie-Von Schweidler given by:

$$I = At^{-n} \quad (1)$$

where  $A$  is an empirical parameter and  $n$  is the exponent of the power law. The exponent  $n$  can be obtained from the slope of the transient current in a bilogarithmic plot. A value of  $n$  close to 1 often involves the orientation of dipoles in the direction of the electric field. On the contrary, when  $n$  becomes close to 0, this indicates that the steady-state current is reached and that most of the current is due to charge carrier motion and no more to dipole contribution.

Table 1 summarizes the different values of the exponent  $n$  obtained by fitting the transient currents for the different fields and temperatures with the Curie-Von Schweidler law. At 200  $^\circ\text{C}$  for fields beyond 1600  $\text{kV}/\text{cm}$ , the value of  $n$  appears lower than 0.35 which indicates that in these conditions a slight contribution of dipolar current is present in the first stage of the polarization currents. However, for higher fields, the lower values of the exponent mean that the main contribution of the current is due to mobile charges (conduction currents).

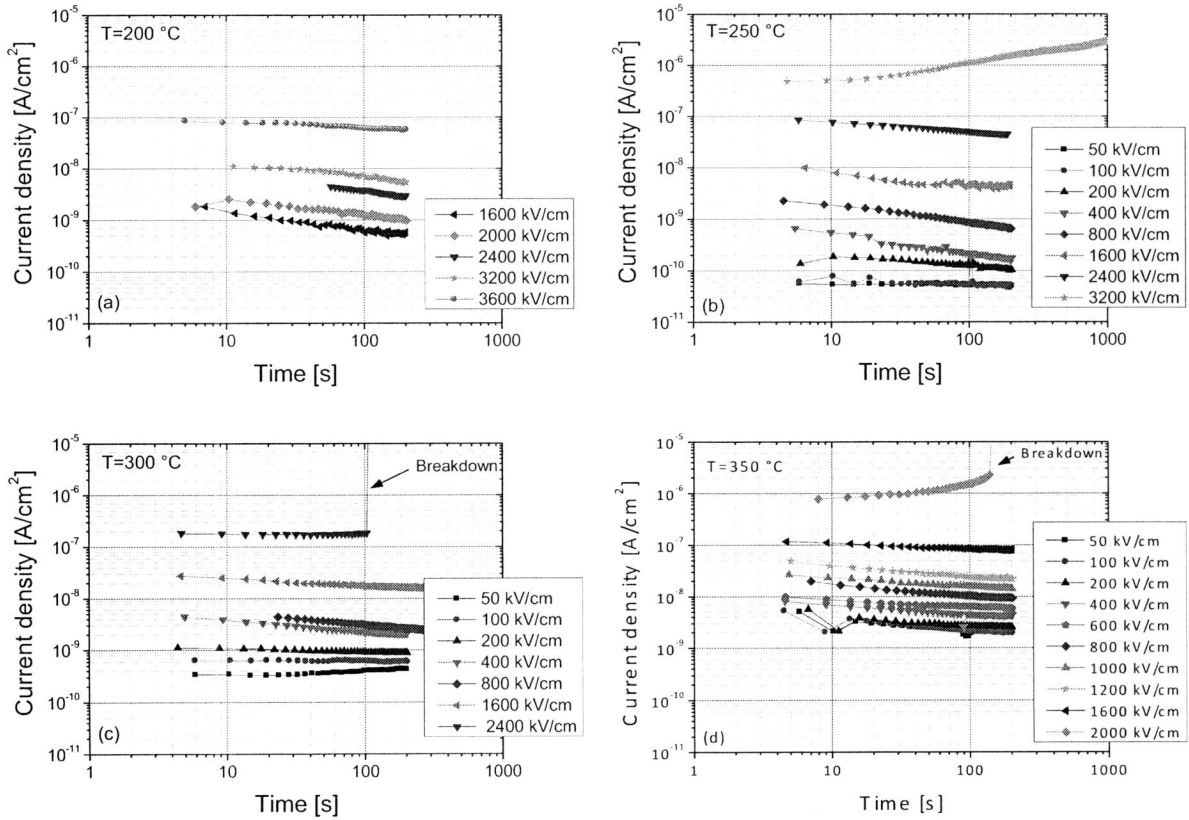


**Figure 3.** Transient current density in PA-HT films versus time and for different applied electric fields at 200 °C (a), 250 °C (b), 300 °C (c) and 350 °C (d). (Film thickness: 1.2  $\mu\text{m}$ ).

For higher temperatures ( $\geq 250$  °C), the conduction current appears directly as the main part of the current as soon as the beginning of the polarization (low values of  $n$ ).

A last observation is the occurrence of an abnormal increase in the transient currents for the extreme applied electric fields. Indeed, at 250 °C and for 3200 kV/cm, the transient current exhibits an increase typical of the formation of a space charge within the polymer bulk. The formation of such a space charge (in the case of a heterocharge) usually leads to field reinforcements in the vicinity of the interfaces with electrodes.

At 300 °C and 350 °C, the formation of this space charge occurs for lower fields (2400 kV/cm and 2000 kV/cm respectively). Moreover, in these cases where both temperature and field are very high, the abnormal currents end by the breakdown of the PA-HT films after only 100-150 seconds.

### 3.2 CURRENT-FIELD CHARACTERISTICS

Figure 4 shows the conduction current density (extracted from the steady state region) versus electric field in PA-HT for different temperatures between 200 °C and 350 °C.

It is possible to observe on these curves the occurrence

of two main conduction regions: (i) a quasi ohmic conduction region and (ii) a strong non-linear region where the current increases quickly with the electric field.

**Table 1.** Evolution of the exponent  $n$  of the Curie-Von Schweidler law (eq. (1)) with field and temperature.

Field (kV/cm)	Values of the exponent $n$			
	200 °C	250 °C	300 °C	350 °C
50	-	0.030	0.017	0.170
100	-	0.073	0.023	0.191
200	-	0.175	0.069	0.136
400	-	0.369	0.205	0.157
500	-	-	-	-
600	-	-	-	0.118
800	-	0.349	0.241	0.204
1000	-	-	-	0.167
1200	-	-	-	0.198
1600	0.339	0.184	0.128	0.098
2000	0.264	-	-	SC+BD
2400	0.348	0.190	SC+BD	-
3200	0.281	SC	-	-
3600	0.125	-	-	-

SC: space-charge abnormal current; BD: breakdown.

The threshold field is near 1000 to 1500 kV/cm for all the temperatures. As discussed above, the super non-linear region at very high field can be easily attributed to space-charge limited currents (SCLC) phenomena supported by the presence of abnormal currents during the transient phase. Moreover, the slopes of the  $j$ - $F$  curves (slope  $>2$ ) are in agreement with the SCLC mechanism. Recently, we have reported such kind of electrical conduction in thin polyimide (PI) films in a similar temperature range highlighting the complete characteristic of SCLC [10]. In the case of PI films, the transient currents are also characterized by the occurrence of abnormal currents [11], as in the present study.

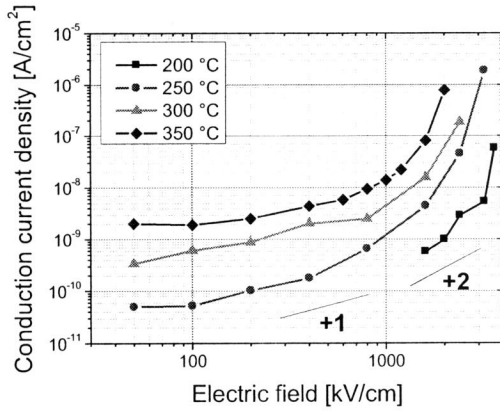


**Figure 4.** Conduction current density versus electric field of PA-HT for different temperatures.

In the case of PA-HT, as we have only observed the beginning of the super non-linear region (slope  $>2$ ) of the conduction currents, in the following we will only focus and discuss the conduction mechanisms in both the ohmic and low injection field regions (slopes of +1 and +2).

### 3.3 CONDUCTION MECHANISM STUDY

Among the macroscopic theories describing the injection phenomena from the metal contact, the Schottky theory is the more advanced up to now to describe how a charge is introduced in dielectrics with the help of temperature and field. The Schottky model describes the field dependent lowering of the triangular potential barrier for thermoionic injection [12,13]. In this case, the charge injection from the electrode into the insulator is governed by the relation:

$$j = A_{RD} T^2 \exp\left(-\frac{\phi_0 - \beta_S \sqrt{F}}{kT}\right) \quad (2)$$

with

$$\beta_S = \sqrt{\frac{q^3}{4\pi\epsilon_r\epsilon_0}} \quad (3)$$

where  $A_{RD}$  is the Richardson-Dushman's constant,  $k$  is the Boltzmann's constant,  $\beta_S$  is the Schottky's constant,  $\epsilon_r$  and  $\epsilon_0$  are respectively the dielectric constant and vacuum permittivity,  $q$  is the electronic charge,  $\phi_0$  is the effective work function between the Fermi level of the electrode and the conduction band of the insulator in the absence of field ( $F=0$ ).

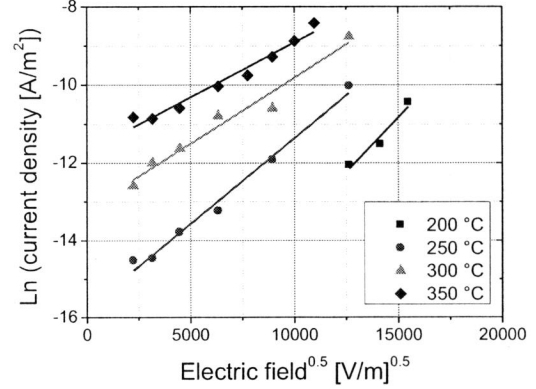


**Figure 5.**  $\ln j$ - $F^{1/2}$  plot for different temperatures. Solid lines represent the best fits in the linear regions.

Figure 5 presents the plot of  $\ln j$  versus  $F^{1/2}$  of the conduction currents below the threshold field for the different temperatures. Between 200 °C and 350 °C, the results can be fitted by straight lines given by Eq. (2). A mean to validate if the Schottky effect is involved in the conduction process for the temperature and field ranges under investigation is to compare the dielectric constant evaluated through the slope  $\beta_S/k_B T$  of each straight line with the theoretical value for PA-HT.

The values of the dielectric permittivity  $\epsilon_r$  obtained from the straight lines are given in Table 2. These permittivity values have to be compared with the theoretical high frequency dielectric constant  $\epsilon_{theo} \approx 2.4$  of the PA-HT thin films in the same temperature range [7]. Strong deviations of  $\epsilon_r$  from the theoretical permittivity value would lead to exclude a pure Schottky injection mechanism. Between 200 °C and 350 °C, the derived values of  $\epsilon_r$  are in the range from 2.74 to 6.43. These values are largely higher than  $\epsilon_{theo}$  of PA-HT. The ratio  $\gamma = \epsilon_{theo} / \epsilon_r$  corresponds to the field-distortion factor in the vicinity of the injecting electrode induced by the charge pile-up [14]. This dimensionless parameter corresponds to the presence at the interface contact of a homocharge if  $\gamma < 1$  and a heterocharge for  $\gamma > 1$  [15]. In the present case, the field-distortion factor is in the order of 0.88-0.37, i.e. below from 1 which leads to highlight homocharge field distortion below the threshold field. It is interesting to observe that  $\gamma$  decreases with increasing temperature leading to show an increase of homocharge injection. Moreover, an increase of the effective work function  $\phi_0$  has been obtained with increasing temperature from the fits at zero-field intercepts which is contradictory with theory. All these results allow

reasonably excluding the participation of the Schottky effect in the electrical conduction of PA-HT.

Let us notice that far beyond the threshold field ( $\gg 1500$  kV/cm) the slopes have indicated a change in  $\gamma > 1$  corresponding to a progressive switch from a homo space-charge to a hetero space-charge (not presented here), in agreement with the abnormal currents shown in Figure 3.

**Table 2.** Physical parameters obtained from the fits with the Schottky and Poole-Frenkel models.

Temperature	200 °C	250 °C	300 °C	350 °C	
$\beta \times 10^{24}$ (J m <sup>1/2</sup> V <sup>-1/2</sup> )	3.676	3.179	2.674	2.398	
Schottky	$\epsilon_r$ (from $\beta_S/kT$ )	2.74	3.66	5.17	6.43
	$\gamma_S = \epsilon_{theo}/\epsilon_r$	0.88	0.66	0.46	0.37
	$\phi_0$ (eV)	1.79	1.91	1.97	2.07
Poole-Frenkel	$\epsilon_r$ (from $\beta_{PF}/kT$ )	10.94	14.62	20.67	25.71
	$\gamma_{PF} = \epsilon_{theo}/\epsilon_r$	0.22	0.16	0.12	0.09

Among the bulk conduction theories, the Poole-Frenkel model describes how ‘electronic-type’ carriers are released from neutral donor or acceptor levels (i.e. ionized donors or acceptors) when the coulombic potential barrier is lowered by the applied electric field [13,16]. The carriers are then band transported [Tess05]. The potential wells (or localized states) correspond also to recombination sites charged when no carrier is trapped there. In this case, the current density in the insulator containing shallow traps is given by:

$$j = j_0 \exp\left(-\frac{\phi_{PF0} - \beta_{PF}\sqrt{F}}{kT}\right) \quad (4)$$

with 
$$\beta_{PF} = \sqrt{\frac{q^3}{\pi\epsilon_r\epsilon_0}} = 2\beta_S \quad (5)$$

where  $j_0$  is the pre-exponential current density,  $\phi_{PF0}$  is the trap barrier height when  $F=0$  and  $\beta_{PF}$  is the Poole-Frenkel’s constant which is twice the Schottky one.

The slopes of  $\ln j$  versus  $F^{1/2}$  in Figure 5 for the different temperatures yield to values of  $\epsilon_r$  between 14.62 and 25.71 largely outside of the expected range close to 2.4 (see Table 2). Such strong deviations allow excluding a Poole-Frenkel conduction as well. The Schottky and Poole-Frenkel conduction models produce unrealistic and significantly higher values of the dielectric constant of PA-HT, which can indicate the development of homo-type space-charge at the electrodes below the threshold field. However, the data obtained in this study does not follow ideal SCLC behavior and this deviation may be explained by the influence of trapping.

‘Hopping’ refers to transport mechanisms that do not involve the conduction band for electrons (or the valence

band for holes) [Tess05]. Since variable range hopping (VRH) conduction cannot be involved at high temperature by tunneling effect from one state to another [17,18], in the following, the conduction current results are thus analyzed and interpreted on the basis of the thermally assisted hopping (TAH) conduction theory. In TAH model, the transport is controlled by neutral traps. The carriers (electronic-type or ions) gain energy through random thermal fluctuations or phonon interaction to escape their localized state, overcome the potential barrier, travel in an extended state for a small amount of time before being recaptured by another localized state [17]. The theoretical current for TAH is given by [18]:

$$j = 2qN\lambda\nu \exp\left(-\frac{U}{kT}\right) \sinh\left(\frac{q\lambda F}{2kT}\right) \quad (6)$$

where  $N$  is the free carrier density,  $\lambda$  is the apparent hopping jump distance between two active traps,  $\nu$  is the vibration frequency of carriers and  $U$  is the average trap depth ( $F=0$ ). Under the assumption of high field approximation ( $q\lambda F \gg 2kT$ ), Eq. (6) can be written as follows:

$$j = j_0 \exp\left(\frac{q\lambda F}{2kT}\right) \quad (7)$$

where  $j_0$  is the zero-field current density given by:

$$j_0 = 2qN\lambda\nu \exp\left(-\frac{U}{kT}\right) \quad (8)$$

Figure 6 presents the plot of  $\ln j$  versus  $F$  of the conduction currents below the threshold field for the different temperatures. Between 200 °C and 350 °C and in the high field region, the results can be fitted by straight lines given by Eq. (7). The slope of the straight lines gives the hopping jump distance  $\lambda$ .

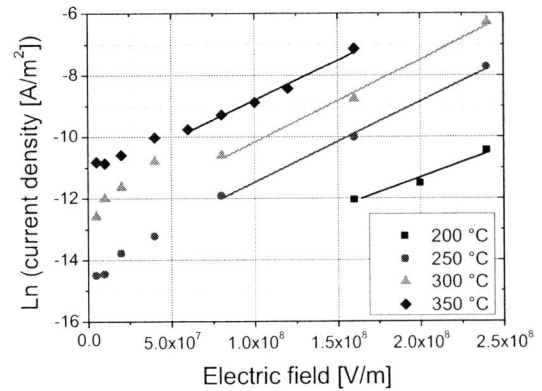


**Figure 6.**  $\ln j$ - $F$  plot for different temperatures. Solid lines represent the best fits in the linear regions.

The values of the hopping jump distance are summarized in the Table 3. The value of  $\lambda$  ranges from 16

Å to 29 Å with increasing from 200 °C to 350 °C. However, the hopping distance exhibits saturation from 250 °C.

**Table 3.** Hopping jump distance versus temperature.

Temperature	200 °C	250 °C	300 °C	350 °C
$\lambda$ (Å)	16	24	27	29

Those values of  $\lambda$  are in good agreement with data obtained by Kahouli *et al* in another type of parylene films [19]. However in their case, as in other polymers, an increase of  $\lambda$  with increasing temperature is observed [20,21]. The origin of such an increase of the hopping jump distance remains sometimes misconceived.

In polymers with ionic hopping conduction, Kosaki *et al* have reported earlier that the glass transition plays an important role in the increase in  $\lambda$  [20]. They described that the configuration of the polymer chains in the amorphous phase constitutes large potential barriers trapping neutral or charged particles. Below the glass state, where the motions of the main chains are frozen, the migration of carriers (particularly ions) can be blocked by very high barriers introduced by the crystalline regions. In the glass transition region, micro-Brownian motions are liberated gradually and the high potential barriers which restricted the migration of ions may disappear or change their position temporally or spatially. Therefore, the elongation of the hopping jump distance may be associated with the effective evanescence of the high barriers [20].

On the contrary, in polymers with electronic-type hopping conduction (i.e. crystalline ones), electrons move rapidly through lamella and in free volume around lamella surfaces, while holes move rapidly through lamella and along lamella surfaces. Therefore, the amorphous regions act as transport ‘blockages’ for electronic carriers and electronic charge transport appears as a structured process on the sub-micron scale [22].

Most of the polymers (amorphous or crystalline) exhibit hopping jump distances from less than 1 nm up to 20 nm with among them a large amount ranging from 1 to 6 nm. So, it is difficult to conclude definitively on the nature of the charge carriers only on the basis of the hopping jump distance value. However, general tendencies can be drawn: (i) in the case of ionic hopping,  $\lambda$  sharply rises near the glass transition ( $T_g$ ) to reach larger values of several nm up to >10 nm; (ii) for electronic hopping, it seems difficult to envisage charge travelling along very large distances (>10 nm) due to the need for charges to hop in an organized molecular structure, moreover, the development of free voids (due to  $T_g$ ) should act as barrier against such kind of hopping; (iii) for  $\lambda$  values ranging 0.5-2 nm, it is complicated to conclude since such distances correspond both to the size of lots of monomer units and distances between chains (i.e. interplanar distance between two lamellae in the crystalline phase or parts of free-volume in the amorphous phase).

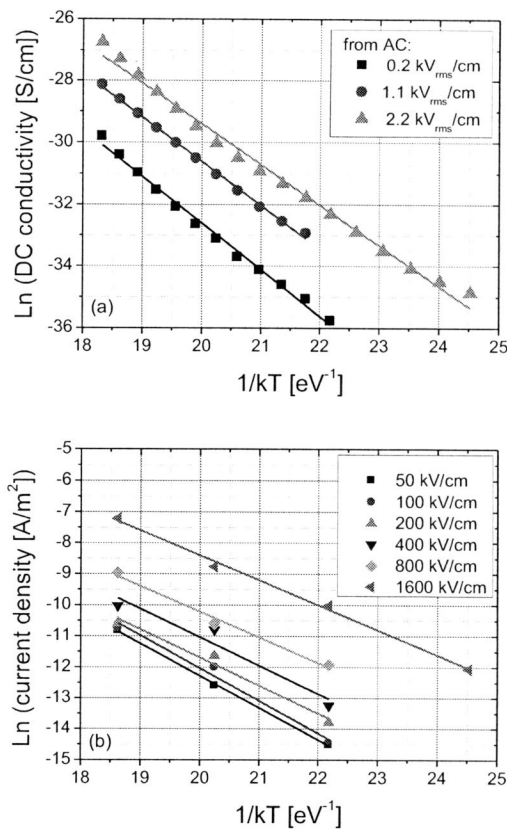


**Figure 7.** Reciprocal temperature dependence of the DC conductivity measured by dielectric spectroscopy under low AC fields (a) and of  $\ln j$  for different high DC fields (b). Solid lines represent the best fits.

In the present case, the hopping jump distances  $\lambda$  are in a range where it is difficult to conclude without complementary analyses.

To support electronic-type hopping (i.e. structured transport), it is necessary to look at both the dimensions of the PA-HT monomeric units and the distance between parallel lamella in the crystalline phase. Park *et al* have reported in similar parylene F-type that the material owns a triclinic configuration unit cell containing one monomer with dimensions of  $a=5.36$  Å,  $b=5.92$  Å,  $c=6.57$  Å (chain axis) [23]. These unit dimensions are independent of the material phase (amorphous or crystalline). Moreover, in our previous works for annealed PA-HT films, an interplanar spacing between lamella (in the crystalline phase) of 4.3 Å has been reported [6-8]. Those values are largely lower than the hopping jump distance. This could exclude an electronic-type hopping due to incompatible (from a theoretical point of view) intramolecular or intermolecular transport distances. Moreover, the predictions to be in presence of a homo-space-charge near the electrodes support this assumption. However, before to conclude definitely on the absence of this kind of transport it will deserve complementary analyses such as space-charge measurements.

On the other hand, to support ionic-type hopping a discussion regarding the hopping distance needs to be done.

Indeed, semi-crystalline PA-HT films present a low glass transition temperature ranging 16 to 100 °C [7]. In the present case, all the measurements are performed above  $T_g$  and it is observed a slight increase of  $\lambda$  between 200 and 250 °C and then its saturation up to 350 °C. This result is in agreement with those of Kosaki *et al* in PVC and Amborski in PET where  $\lambda$  saturates well above  $T_g$  [20,29]. PA-HT films seem presenting the same feature characteristic of ionic-type hopping insulating.

In order to identify potential origins of ionic species responsible of the hopping conduction, it is necessary to look at physico-chemical analyses of the material and its interfaces. In fluorinated parylenes, Senkevich *et al* showed by XPS that broken C–F bonds and the formation of the metal-F bonding may be the source of fluorine diffusion in metal electrodes, such as Al and TaN<sub>x</sub> [24]. They also showed that a metal-oxide overlayer (Al<sub>2</sub>O<sub>3</sub>) can stop fluorine diffusion in the metal. Shi *et al* observed in Teflon very little defluorination even with noble metals (Au and Ag) with the formation of AuF<sub>x</sub> bondings [25]. Based on these results, Kahouli *et al* have recently evocated that fluorine species could be at the origin of high temperature space charge relaxation in parylene AF4 due to defluorination with reactive metals [26]. Probable trapping and detrapping of fluorine anions (F<sup>-</sup>) inside the material at the interfaces could occur. They estimated a hopping barrier height for the conduction near 1.20 eV from AC conductivity measurements, which they attributed to F<sup>-</sup> transport. Earlier, other work of Félix-Vandorpe *et al* reported on polyvinylidene fluoride (PVDF) also highlighted the localization of fluorine under the electrodes when the material is subjected to an alternating voltage of low amplitude at temperatures from 100 to 130 °C [27]. They as well have observed (through retrodiffusion experiments) that F<sup>-</sup> anions driven by the field are extracted out of the bulk through the metal electrodes. Thus, they have excluded their blockade at the interfaces and their contribution to space charge, contrary to Kahouli's conclusions. However, they involved second ionic specie (H<sup>+</sup>) which could be blocked at interfaces and so could play a key role in the conduction to fully explain their electrical results. Indeed, the activation energy they found (1.2 eV) corresponds perfectly to the sum of those of the carrier density and mobility for H<sup>+</sup> ions, which was not the case for F<sup>-</sup> anions. All these works show the presence of F<sup>-</sup> anions and probable H<sup>+</sup> protons near the metal-polymer interfaces and their effects (under AC fields) on the hopping conduction in various fluorinated polymers.

Figure 7 presents the Arrhenius plots of the DC conductivity (extracted from AC measurements at different low fields, not shown here) and of the DC conduction currents for different DC fields. From the slopes of the different fitted curves, a field-dependant activation energy is obtained corresponding to the evolution of the hopping barrier height (or trap depth) when this latter is lowered (see Figure 8). It is observed that when the field is close to zero (AC measurements), the hopping barrier height reaches value above 1.5 eV corresponding to very deep traps typical of ions [ref]. Such barrier heights are slightly higher than

those obtained for F<sup>-</sup> ions hopping in PA-AF4 films [26]. In the present case, this can be explained through the fact that the PA-HT films have been annealed before measurements in order to increase the crystallization rate and stabilize their electrical properties at high temperature. Actually, we reported earlier that such a curing allows strongly reducing the Maxwell-Wagner-Sillars bulk interfacial polarization [7]. Consequently, the mobility of charge carriers in the amorphous phase was reduced. In Figure 7b, at higher electric fields, the slopes of the fits performed on  $\ln j(1/kT)$  corresponds to the apparent hopping barrier height when this latter is distorted by the field. The obtained slopes still decrease with field increasing showing the decrease of the barrier height that ions have to overcome to be detrapped. As the field increases up to 1000 kV/cm, the barrier height is progressively reduced down to 0.80 eV with a good continuous tendency curve between the two ways of measurement. Considering that the hopping jump distance is constant in the range 200–350 °C (see Table 3), it seems that the increase in the conduction current magnitude is preferentially due to charge carriers multiplication in the conduction band (due to hopping barrier reduction) and not to an increase of their mobility.

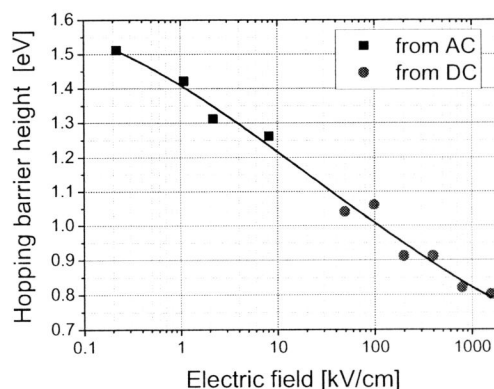


**Figure 8.** Evolution of the hopping barrier height in PA-HT with the applied electric field.

### 3.4 PA-HT THICKNESS EFFECTS

Figure 9 presents the PA-HT thickness effect on the conduction current density versus electric field at 300 °C and 350 °C. It is shown that the thickness effect is not significant. This is most probably due to the VDP process that does not require any solvent. This confirm that in this field range (below the threshold field), the measured currents for the 1.2 and 4.9 μm films are not due to SCLC phenomenon (heterocharge) for which the current density must be proportional to the inverse of the film thickness.

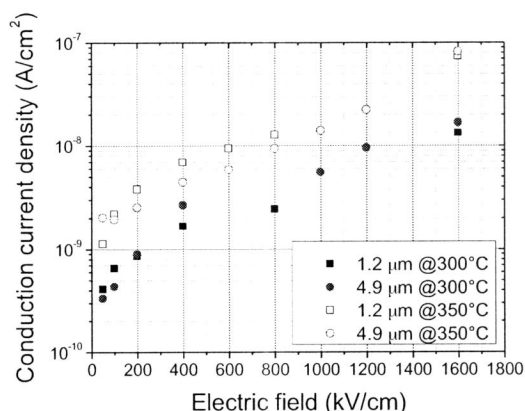


**Figure 9.** Effect of the PA-HT thickness on the conduction current density versus electric field at 300 °C and 350 °C.

### 3.4 POLARITY EFFECTS AT HIGH FIELD

Figure 10 presents the effect of the electric field polarity on the conduction current density at 200 °C and in the very high field range.

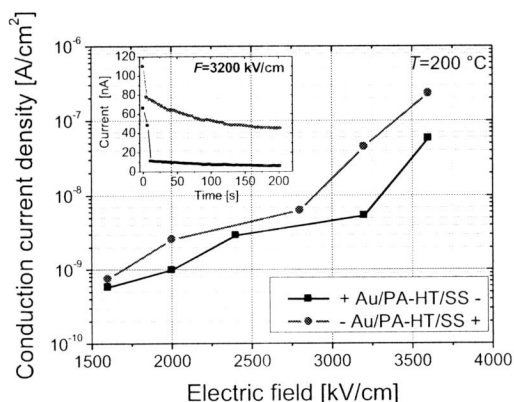


**Figure 10.** Effect of the electric field polarity on the conduction current density in PA-HT (1.2 μm) at 200 °C in the very high field range. The inset figure shows an example of the transient currents at 3200 kV/cm for the two polarities.

Whereas an independence of the polarity was observed below 1500 kV/cm, a difference in the current density is observed at fields higher than 1600 kV/cm and the positive gold polarization electrode shows a lower current density than stainless steel one. Since the gold owns a higher work function (5.1-5.4 eV) than stainless steel (4.4 eV), and if electrons were the main contributing carriers, a higher current should be observed when the gold electrode is positively polarized (anode). However, in the present case, an opposite behavior is observed indicating that the holes contribution to the injection at very high field is very significant. Such implication of a hole injection has also been reported in non fluorine parylene [28] and in many others fluorinated polymers as well [30,31]. It has been demonstrated that the polarity of dominant carriers changes from negative to positive as the fluorine substitution increases. Fluorine atoms are electronegative and they may

provide deep electron traps, which suppress the current due to negative carriers and can explain why positive carriers dominate the current in fluorinated parylene for electric fields higher than 1500 kV/cm. This suggests that better insulation at high field can be obtained by using electrodes with lower work functions.

## 5 CONCLUSION

The electrical conduction of fluorinated parylene (PA-HT) was investigated at high temperature in the range from 200 to 350 °C, for electric fields between 50 and 3600 kV/cm and for thicknesses from 1.2 to 11 μm. A decrease in the current during the bias time was observed and was related to slight dipolar orientation. Steady-state currents were investigated by assuming different conduction models. The thermally assisted hopping (TAH) mechanism appears as the most probable conduction model for fields up to the threshold (1500 kV/cm). Based on the analysis of the hopping jump distance and its evolution versus temperature, an ionic hopping conduction could be the most adequate origin to describe our results. A discussion on the nature of the ionic carriers is carried out. The activation energy of hopping conduction is field dependent and decreases with field increasing indicating the progressive detrapping of the carriers. The film thickness shows a good correlation with previous works. Finally, the electrode effects at high fields (>1500 kV/cm) shows lower conduction currents when the electrode owning the higher work function is positively biased indicating that positive carriers (holes) are the main contributors to the injection current.

## ACKNOWLEDGMENT

The authors warmly thank the financial support brought to this work by the General Directorate of Armaments of the French Ministry of Defense (DGA) and the General Directorate of Competiveness, Industry and Services of the French Ministry of Productive Recovery (DGCIS). The authors are also very grateful to Specialty Coating Systems, Inc. (SCS) for supplying the Parylene HT films.

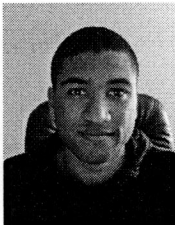
## REFERENCES

- [1] H. Treichel, G. Ruhl, P. Ansmann, R. Würll, C. Müller and M. Dietlmeier, "Low dielectric constant materials for interlayer dielectric", *Microelectronic Engineering*, Vol. 40, No.1, pp. 1-19 1998.
- [2] S. Lavina, E. Negro, G. Pace, S. Gross, G. Depaoli, M. Vidali and V. Di Noto, "Dielectric low-k composite films based on PMMA, PVC and methylsiloxane-silica: Synthesis, characterization and electrical properties", *Journal of Non-Crystalline Solids*, Vol. 353, No. 30-31, pp. 2878-2888, 2007.

- [3] K. L. Mittal, *Polyimides: Synthesis, Characterization and Applications, I and II*. (New York: Plenum Press), 1984.
- [4] W. F. Beach, C. Lee, D. R. Bassett, T. M. Austin and R. Olson, *Xylylene Polymers*, in *Encyclopedia of Polymer Science and Engineering*, 2<sup>nd</sup> Ed. 17, (New York: J. Wiley & Sons), 1991.
- [5] W. R. Dolbier Jr. and W. F. Beach, "Parylene-AF4: a polymer with exceptional dielectric and thermal properties", *Journal of Fluorine Chemistry*, Vol. 122, pp. 97-104, 2003.
- [6] S. Diaham, M. Bechara, M.-L. Locatelli and C. Tenailleau, "Electrical conductivity of parylene F at high temperature", *Journal of Electronic Materials*, Vol. 40, No. 3, pp. 295-300, 2011.
- [7] S. Diaham, M. Bechara, M.-L. Locatelli and T. Lebey, "Influence of crystallization-induced amorphous phase confinement on  $\alpha$ - and  $\beta$ -relaxation molecular mobility in parylene F", *Journal of Applied Physics*, Vol. 110, pp. 063703, 2011.
- [8] S. Diaham, M. Bechara, M.-L. Locatelli, R. Khazaka, C. Tenailleau and R. Kumar, "Dielectric Strength of Parylene HT", *Journal of Applied Physics*, Vol. 115, No. 5, pp. 054102, 2014.
- [9] J. K. Fink, Chap. 2 in *High Performance Polymers* (William Andrew Publishing, Norwich, New York), 2008.
- [10] S. Diaham and M.-L. Locatelli, "Space-charge-limited currents in polyimide films", *Applied Physics Letters*, Vol. 101, pp. 242905, 2012.
- [11] S. Diaham and M.-L. Locatelli, "Time and frequency domains dc conductivity analysis in thin dielectric films at high temperature", *Journal of Physics D: Applied Physics*, Vol. 44, pp. 105402, 2011.
- [12] G. M. Sessler, B. Hahn and D. Y. Yoon, "Electrical conduction in polyimide films", *Journal of Applied Physics*, Vol. 60, pp. 318, 1986.
- [13] H. J. Wintle, Chapter 6 in *Engineering Dielectrics Vol. II-A* (ed. R. Barhikas and R. M. Eichorn, Philadelphia, pp. 588-600), 1983.
- [14] G. Lengyel, "Schottky emission and conduction in some organic insulating materials", *Journal of Applied Physics*, Vol. 37, pp. 807-810, 1966.
- [15] A. Krivda *et al*, "Characterization of epoxy microcomposite and nanocomposite materials for power engineering applications", *IEEE Electrical Insulation Magazine*, Vol. 28, pp. 38-51, 2012.
- [16] J. G. Simmons, "Conduction in thin dielectric films", *Journal of Physics D: Applied Physics*, Vol. 4, pp. 613-657, 1971.
- [17] J. R. Dennison and J. Brunson, "Temperature and Electric Field Dependence of Conduction in Low-Density Polyethylene", *IEEE Transactions on Plasma Science*, Vol. 36, No. 5, pp. 2246-2252, 2008.
- [18] J. Brunson, "Hopping Conductivity and Charge Transport in Low Density Polyethylene", PhD Thesis, Utah State University, 2010.
- [19] A. Kahouli, F. Jomni, A. Sylvestre, B. Yangui and J. Legrand, "I-t, J-I/T and J-E characteristics for the understanding of the main mechanism of electric conduction and the determination of the glass transition temperature of parylene C thin films", *Journal of Physics D: Applied Physics*, Vol. 44, pp. 505302, 2011.
- [20] M. Kosaki, K. Sugiyama and M. Ieda, "Ionic jump distance and glass transition of polyvinyl chloride", *Journal of Applied Physics*, Vol. 42, pp. 3388-3392, 1971.
- [21] A. A. Alagiriswamy, K. S. Narayan and Govinda Raju, "Relaxation processes in aromatic polyimide", *Journal of Physics D: Applied Physics*, Vol. 35, pp. 2850-2856, 2002.
- [22] Y. Zhao, A. S. Vaughan, J. V. Champion, S. J. Dodd and S. J. Sutton, "The structure of trees in semi-crystalline polymers", *Proceedings of 8<sup>th</sup> International Conference on Dielectric Materials, Measurements and Applications (DMMA)*, pp. 314-319, 2000.
- [23] S.-Y. Park, J. Blackwell, S. N. Chvalun, K. A. Mailyan, A. V. Pebalk and I. E. Kardash, "A three-dimensionally oriented texture for poly( $\alpha,\alpha,\alpha',\alpha'$ -tetrafluoro-*p*-xylylene)", *Macromolecules*, Vol. 32, pp. 7845-7852, 1999.
- [24] J. J. Senkevich, B. Wang, J. B. Fortin, M. C. Nielsen, J. F. McDonald, T.-M. Lu, G. M. Nuesca, G. G. Peterson, S. C. Selbrede, M. T. Weise, "Stability of Fluorinated Parylenes to Oxygen Reactive Ion Etching under Aluminum, Aluminum Oxide, and Tantalum Nitride Overlayers", *Journal of Electronics Materials*, Vol. 32, pp. 925-931, 2003.
- [25] M. K. Shi, B. Lamontagne, A. Selmani, L. Martinu, E. Sacher, M.R. Wertheimer, and A. Yelon, "Metallization of Teflon PFA. II. Interactions of Ti, Ag, and Au measured by x-ray photoelectron spectroscopy", *Journal of Vacuum Science and Technology A*, Vol. 12, pp. 807-, 1994.
- [26] A. Kahouli, A. Sylvestre, F. Jomni, E. André, J.-L. Garden, B. Yangui, B. Berge, and J. Legrand, "Dielectric Properties of Parylene AF4 as Low-*k* Material for Microelectronic Applications", *Thin Solid Films*, Vol. 520, pp. 2493-2497, 2012.
- [27] M. C. Félix-Vandorpe, M. Maitrot and R. Ongaro, "Electrical properties at very low frequencies of alpha PVDF subjected to thermal cycling", *Journal of Physics D: Applied Physics*, Vol. 18, pp. 1385-1399, 1985.
- [28] T. Mizutani, T. Mori, Y. Yakai and M. Ieda, "High field conduction in poly-*p*-xylylene thin film", *Conference Record of the IEEE International Symposium on Electrical Insulation*, pp. 154-154, June 5-8, Boston, MA, 1988.
- [29] Amborski.

- [30] T. Mizutani, S. Ikeda and M. Ieda, "Influence of chemical structure on electrical conduction in insulating polymers", *Japanese Journal of Applied Physics*, Vol. 24, No. 9, pp. 1164-1167, 1985.
- [31] M. Ieda, T. Mizutani and S. Ikeda, "Electrical conduction and chemical structure of insulating polymers", *IEEE Transactions on Electrical Insulation*, Vol. EI-21, No. 3, pp. 301-306, 1986.

A. Okoniewski and M. M. Perlman, "Hopping conduction in "pure" polypropylene", *Journal of Polymer Science Part B: Polymer Physics*, Vol. 32, pp. 2413-2420, 1994.



**Sombel Diahm** was born in Montauban, France, in 1982. He received his M.Sc. degree and PhD degree in Electrical Engineering, respectively in 2005 and 2007, both from the Paul Sabatier University of Toulouse, France. In 2005, he joined the LAPLACE laboratory in Toulouse where he becomes, since 2008, Associate-Professor. His current research fields focus on the study of dielectric materials for the insulating

environment (passivation and encapsulation) of high temperature and/or high voltage wide band gap semiconductor power devices (SiC, GaN and Diamond). His fields of interest cover from both the study of the physical properties of insulating materials and their reliability in high temperature, up to the study of their impact on the electrical characteristics of the devices. He is co-author of 6 communications in international scientific reviews and 8 papers in international conferences.



**Marie-Laure Locatelli** was born in Nantua, France, in 1965. She received the Engineering degree in Electrical Engineering in 1988 and the PhD degree in Integrated Electron Devices in 1993 from the INSA of Lyon (France). As a Research Associate of the National Center of Scientific Research (CNRS) since 1993, she had been working at CEGELY Laboratory in Lyon for 8 years, on the study of silicon power device high temperature limitations, and on the study of new

SiC power devices. Since 2001, she has been working at the LAPLACE laboratory in Toulouse. She studies dielectric materials suitable for the insulating environment of high temperature and/or high voltage wide band gap semiconductor dies (SiC, GaN and Diamond). She is co-author of 43 communications in international scientific reviews, and 50 papers in international conferences.

## PARYLENE HT FOR ELECTRET GENERATORS

Hsi-wen Lo and Yu-Chong Tai

California Institute of Technology, Pasadena, California, USA

**Abstract:** The use of parylene HT as an electret material is presented. As other parylene variants, deposition of parylene HT is a room-temperature chemical vapor process and parylene HT is MEMS/CMOS process compatible. Compared to Teflon AF, PTFE and CYTOP, parylene HT has much superior charge densities. After corona charging, the highest charge density observed is  $3.69 \text{ mC/m}^2$ , equivalent to a surface potential of  $204.58 \text{ V}/\mu\text{m}$ . A micro power generator with metal rotors and parylene HT electret is developed. The power output is  $5.6 \mu\text{W}$  at  $50\text{Hz}$  with an external load of  $100\text{M}\Omega$ .

**Key Words:** micro power generation, energy harvesting, polymer electret, parylene HT

### 1. INTRODUCTION

Energy scavengers that can harvest waste energy from ambient resources such as natural vibrations, human motions, equipment vibrations and so on have received attention of many researchers in the last decade.

Generally, energy scavengers use two methods to harvest energy from linear vibrations. A piezoelectric harvester uses piezoelectric material to convert strain in the spring into energy [1, 2, 3]. An electromagnetic generator harvests energy by a magnet attached to the proof mass inducing voltages in a coil during linear motion [4, 5].

Most published energy scavengers that harvest energy from linear motions have structures of spring and proof mass. These energy harvesters inherently have resonant frequencies and thus certain narrow bandwidth around the mechanical resonant frequency, while natural harvestable vibration power spectrum usually spans from low to  $\sim 100 \text{ Hz}$  with higher energy in the low frequency end.

To overcome this problem and harvest energy in the low frequency range, new energy harvesters without spring-proof-mass structures has emerged as a solution [6].

### 2. DESIGN OF ELECTRET GENERATOR

Boland et al developed the first design of micro electret power generators without spring proof mass structures [6, 7]. A capacitor-like structure was employed, as shown in Figure 1. Since then, almost all electret power generators use the same design [8, 9]. Power generators taking such

designs inevitably have internal capacitive impedance in addition to external loads.

From Boland et al [7] and Tsutsumino et al [8], the maximum power output can be given as

$$P_{MAX} = \frac{\sigma^2}{4\epsilon_0\epsilon_1 \left( \frac{\epsilon_1 g}{\epsilon_2 d} + 1 \right)} \cdot \frac{dA(t)}{dt} \quad (1)$$

Where  $\epsilon_1, \epsilon_2$  are dielectric constants of electret and air respectively,  $\epsilon_0$  is vacuum permittivity,  $g$  is gap distance between top rotor and electret and  $d$  is the thickness of the electret. From this equation, the maximum power decreases as the gap distance increases. That said, careful and precise gap control is required to achieve high power output.

To eliminate hassles and complexity of gap control, we demonstrated a design that puts two output electrodes on the stator, electret material is applied on the stator and the rotor is a piece of metal to couple both electrodes [10]. Both the rotor and stator are pieces of glass with patterned electrodes and the power is generated when there are relative motions between these two plates, as shown in Figure 2.

However, one drawback of that design is the difficulty to control the movement of the top rotor plate and to keep it in contact with the stator plate during motions. To overcome this, we developed a new design that the rotor is a metal block confined within an external acrylic container. Meanwhile, the metal rotor can keep in contact with the stator all the time by the gravity of the metal mass itself and the coulomb attraction force between charges on the rotor and stator. Figure 3 shows the packaging schematic.

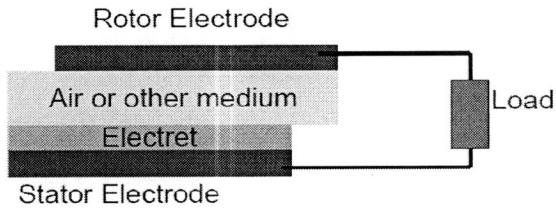


Figure 1. Capacitor-like generator design

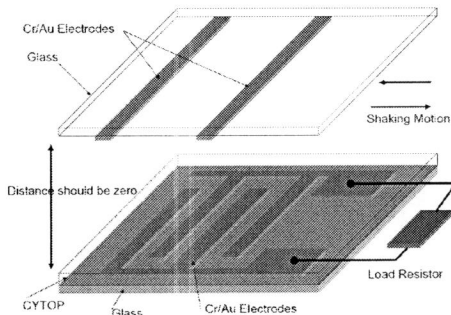


Figure 2. Generators with 2 electrodes on stator

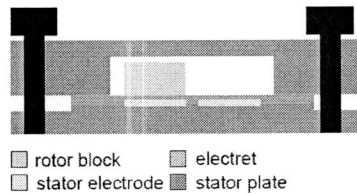


Figure 3. Improved packaging design

### 3. POLYMER ELECTRETS

Many materials have been explored for the use as electret. Hsieh et al demonstrated MEMS electret microphone using Teflon AF [11]. Later on, Boland et al developed a Teflon AF electret power generator [6]. CYTOP was first introduced to micro power generator by Tsutsumino et al [12]. Sterken et al demonstrated a generator using oxide/nitride as electret [9]. Among these explored materials, CYTOP is reported to have highest surface charge density,  $2.8\text{mC/m}^2$  [12].

From Equation 1, the maximum power output of an electret power generator is proportional to the surface charge density squared. Therefore, it is desirable to find an electret material with high surface charge densities. Specialty Coating Systems introduced a new parylene variant, SCS Parylene HT, shown in Figure 4. Like other parylene variants, parylene HT is deposited via a room temperature chemical vapor deposition (CVD) process.

To implant charges onto parylene HT surfaces,

corona charging technique is employed. The optimized corona charging conditions are listed in Table 1. Automatic isoprobe surface potential measurement equipment is used to measure the distribution of the surface potential of parylene HT.

Figure 5 shows the distribution of surface potential per micron of parylene HT. The highest surface potential observed is  $204.58\text{ V}/\mu\text{m}$ , equivalent to a surface charge density of  $3.69\text{ mC/m}^2$ .

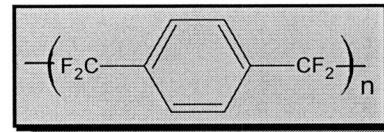


Figure 4. SCS Parylene HT from Specialty Coating Systems.

Base current	$0.02\ \mu\text{A}$
Grid current	$0.2\ \mu\text{A}$
Substrate Temperature	$100\ ^\circ\text{C}$
Charging time	60 minutes

Table 1. Optimized corona charging conditions

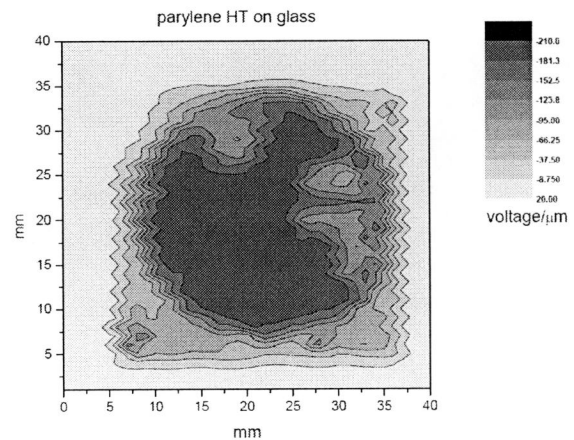


Figure 5. Distribution of surface potential per micron of  $7.32\text{-}\mu\text{m}$  parylene HT film after corona charging.

### 4. DEVICE FABRICATION

The device fabrication starts with soda lime glass wafers.  $2000\text{\AA}$  Au and  $100\text{\AA}$  Cr are thermally evaporated and patterned as the power

output electrodes via conventional photolithographic processes. The electrodes are 5mm by 5mm with 2mm spacing for each cell. Next, the glass wafer is diced into 30mm-by-30mm stators. After dicing, 7.32- $\mu\text{m}$  parylene HT is deposited on the stator. Similar to parylene C and other parylene variant, parylene HT is deposited via the room temperature CVD process. After deposition, corona charging is done to implant charges on parylene HT. Optimized conditions are listed in Table 1.

The rotors are CNC-machined to be 4.5mm by 4.5mm by 2mm (L by W by H) brass blocks. The container is also CNC-machined out of acrylic material. The final assembled device is shown in Figure 6.

### 5. POWER GENERATION

The generator assembly was mounted onto a CNC-machined acrylic stage that is fixed to the electrodynamic shaker. All necessary wires were soldered. Power generation experiments were performed using a Labworks Inc. ET-132-2 electrodynamic shaker, which was driven sinusoidally by a HP33120A function generator through a power amplifier. The acceleration of the power generator was measured using an Endevco256HX-10 accelerometer. The micro electret power generator was connected to a resistive load. In order to measure large output voltages, a simple two-resistor voltage divider was used as the load. The output voltage was measured through a National Semiconductor LF356N op-amp, which is a  $10^{12}$ -ohm input impedance voltage buffer. The shaking amplitude is defined by the external packaging container. For this device, the shaking amplitude is 2mm<sub>p-p</sub>. The frequency is varied from 10Hz to 70Hz and the load resistance from 50Mohm to 2000Mohm.

Figure 7 shows power output as a function of load resistance and Figure 8 shows power output as a function of frequency. Due to the capacitive nature of the device, there is an optimal load for the optimal power generation. Experimentally, it is found to be 100-200 M $\Omega$ , in good agreement with our theoretical prediction. Using the optimal 100 M $\Omega$  load, a maximum power output of 5.6 $\mu\text{W}$  at 50Hz with a sinusoidal-like waveform is produced. Time traces of output voltage are shown in Fig 9.

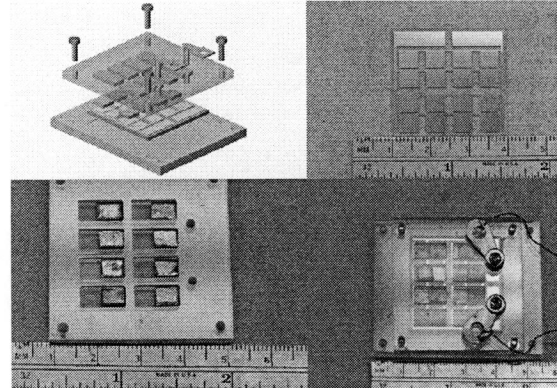


Figure 6. Schematic and photograph of stator, rotor and assembled devices.

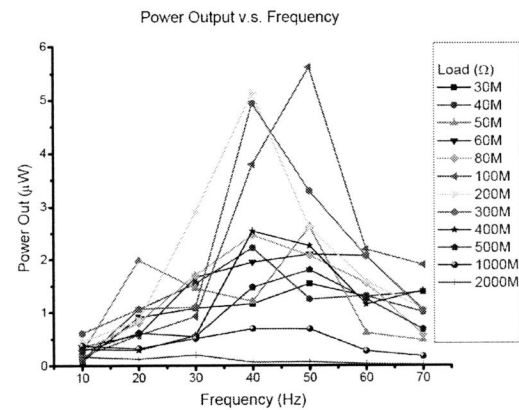


Figure 7. Power output versus frequency

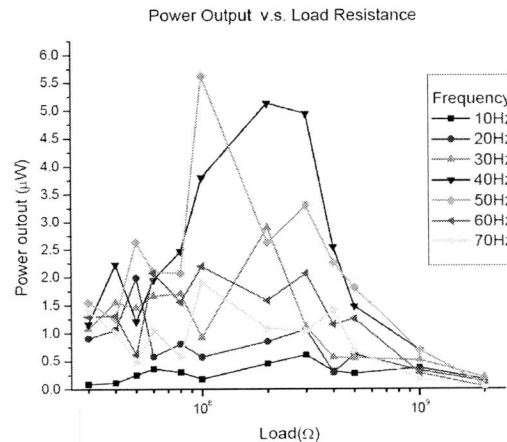


Figure 8. Power output versus load resistance

One important issue of our generator is tearing and wearing problem. After testing, the surface of parylene HT was scratched by the rough surface of poorly-machined brass rotor blocks. The surface potential decreased, too.

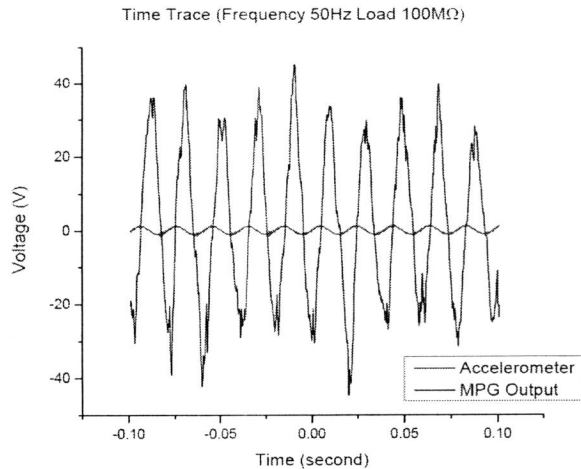


Figure 9. Time traces of voltage output

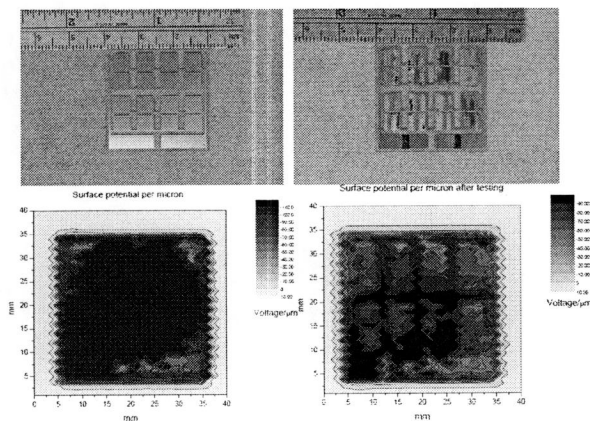


Figure 10. Surface and surface potential of parylene HT before and after testing.

Figure 10 shows the surface of parylene HT and the distribution of surface potential before and after testing. The surface potential dropped from  $100\text{V}/\mu\text{m}$  to around  $60\text{V}/\mu\text{m}$ . This problem can be prevented by carefully polishing the surface of rotor blocks after machining processes.

## 6. CONCLUSION

We demonstrated an improved electret micro power generator. This generator used metal as rotors and both the output electrodes were placed on the stator. With a CNC-machined external packaging container, movement of rotors was confined within fixed ranges.

For the first time, Parylene HT was used as an electret material. Charges were successfully implanted onto parylene HT surfaces via corona charging. The highest surface charge density

observed is  $3.69\text{ mC}/\text{m}^2$ . The maximum power output of this generator is  $5.6\mu\text{W}$  at 50Hz with an external load of  $100\text{M}\Omega$ .

## REFERENCES

- [1] G. K. Ottman, H. F. Hofmann, A. C. Bhatt, and G. A. Lesieutre, "Adaptive Piezoelectric Energy Harvesting Circuit for Wireless Remote Power Supply", *IEEE transaction on Power Electronics*, Vol. 17, No. 5, 2002.
- [2] J. Kymissis, C. Kendall, J. Paradiso, and N. Gerhenfeld, "Parasitic power harvesting in shoes," *Proc. 2nd Int. Symp. Wearable Comput.*, Pittsburgh, PA, Oct. 19–20, 1998, pp. 132–139.
- [3] N. Shenck and J. A. Paradiso, "Energy scavenging with shoe-mounted piezoelectrics," *IEEE Micro*, vol. 21, pp. 30–42, May–June 2001.
- [4] W. J. Li, Z. Wen, P. K. Wong, G. M. H. Chan, P. H. W. Leong, "A Micromachined Vibration-Induced Power Generator for Low Power Sensors of Robotic Systems", *Proc. World Automation Congress: 8th Intl. Symp. on Robotics with Applications*, 2000.
- [5] C. B. Williams, and R. B. Yates, "Analysis of a Micro-electric Generator for Microsystems," *Sensors and Actuators, A*, Vol. 52, 1996, pp. 8–11.
- [6] J. S. Boland and Y. C. Tai, "Liquid-rotor electret micropower generator", *Solid-State Sensor, Actuator, and Microsystems Workshop*, 2004.
- [7] J. Boland, C.-H. Chao, Y. Suzuki, and Y.-C. Tai, "Micro Electret Power Generator," *Proc. Int. Conf. MEMS'03*, 2003
- [8] T. Tsutsumino, Y. Suzuki, N. Kasagi, and Y. Sakane, "Seismic power generator using high-performance polymer electret", *Proc. Int. Conf. MEMS'06*, 2006
- [9] T. Sterken, P. Fiorini, G. Altena, C. Van Hoof, and R. Puer, "Harvesting energy from vibrations by a micromachined electret generator", *Proc. Int. Conf. Transducers 2007*, 2007
- [10] H. Lo, R. Whang, and Y.C. Tai, "A simplified micro electret power generator" *Proc. Int. Conf. MEMS'07*, 2007
- [11] W. H. Hsieh, T. J. Yao, and Y. C. Tai, "A high-performance MEMS thin-film Teflon electret microphone", *Proc. Int. Conf. MEMS'99*, 1999
- [12] T. Tsutsumino, Y. Suzuki, N. Kasagi, and Y. Tsurumi, "High performance polymer electret for micro seismic generator", *Proc. Int. Conf. PowerMEMS2005*, 2005



## Design and Manufacturing of a Double-Side Cooled, SiC based, High Temperature Inverter Leg

Raphaël Riva, Cyril Buttay, Marie-Laure Locatelli, V. Bley, Bruno Allard

► **To cite this version:**

Raphaël Riva, Cyril Buttay, Marie-Laure Locatelli, V. Bley, Bruno Allard. Design and Manufacturing of a Double-Side Cooled, SiC based, High Temperature Inverter Leg. IMAPS. Conference on High Temperature Electronics (HiTEC 2014), May 2014, Albuquerque, United States. pp.THA27. <hal-00997365>

HAL Id: hal-00997365

<https://hal.archives-ouvertes.fr/hal-00997365>

Submitted on 28 May 2014

**HAL** is a multi-disciplinary open access archive for the deposit and dissemination of scientific research documents, whether they are published or not. The documents may come from teaching and research institutions in France or abroad, or from public or private research centers.

L'archive ouverte pluridisciplinaire **HAL**, est destinée au dépôt et à la diffusion de documents scientifiques de niveau recherche, publiés ou non, émanant des établissements d'enseignement et de recherche français ou étrangers, des laboratoires publics ou privés.

# Design and Manufacturing of a Double-Side Cooled, SiC based, High Temperature Inverter Leg

Raphaël RIVA<sup>1</sup>, Cyril BUTTAY<sup>1</sup>, Marie-Laure LOCATELLI<sup>2,3</sup>, Vincent BLEY<sup>2,3</sup>, Bruno ALLARD<sup>1</sup>

<sup>1</sup>Université de Lyon  
CNRS, UMR5005  
INSA-Lyon  
Laboratoire Ampère,  
bâtiment L. de Vinci, 21 avenue Capelle  
F-69621, France  
cyril.buttay@insa-lyon.fr

<sup>2</sup>Université de Toulouse; UPS, INPT; LAPLACE;  
118 route de Narbonne - Bât. 3R3  
F-31062 Toulouse cedex 9, France.  
<sup>3</sup>CNRS; LAPLACE;  
F-31062 Toulouse, France

## ABSTRACT

In this paper, we present a small (25x25x3 mm<sup>3</sup>) power module that integrates two silicon-carbide (SiC) JFETs to form an inverter leg. This module has a "sandwich" structure, i.e. the power devices are placed between two ceramic substrates, allowing for heat extraction from both sides of the dies. All interconnects are made by silver sintering, which offers a very high temperature capability (the melting point of pure silver being 961 °C). The risk of silver migration is assessed, and we show that Parylene-HT, a dielectric material that can sustain more than 300 °C, can completely coat the module, providing adequate protection.

## Keywords

3-D packaging, sandwich module, JFET, silver sintering, silver migration

## 1 Introduction

Silicon Carbide (SiC)-based power devices can in theory operate at very high temperatures (in some cases more than 1000°C, [1]). In reality, many elements (passivation, metal contacts, oxide reliability...) set the maximum temperature of a SiC die to a much lower value, usually 200–400 °C, depending on device. Among the existing SiC power devices, the vertical Junction Field Effect Transistor (JFET) is suited to "high temperature" (300 °C or more) operation [2].

However, although this device was found to withstand continuous operation at 300 °C, that does not mean that it can operate with limited cooling: as was shown in [3], SiC JFETs must be provided with sufficient cooling (2-4 K/W or less) to prevent thermal runaway. There is, therefore, a need for a high temperature package with low thermal resistance.

Double-side cooling, a technique in which heat is removed from both sides of a die, is attractive. It is often implemented in the form of a "sandwich" structure (the die is clamped between two ceramic substrates) [4]. This has the additional advantage of resulting in lower inductance than with classical (wirebonded) power modules [5].

Among the many high temperature bonding solutions [6] that could be used for the assembly of a sandwich

structure, silver sintering is particularly attractive: "low temperature" process (less than 300°C), lead-free, high thermal conductivity (more than 100 W/m.K). It has, however, one major issue: the risk of silver migration [7]. When operating at more than 100 °C, in presence of oxygen and with an electric field, silver atoms tend to migrate and to form conductive filaments across electric potentials, eventually resulting in short circuits.

In addition to this silver migration risk, many other issues had to be addressed to produce a high-temperature capable, silver sintered sandwich power module.

- The SiC JFETs have relatively fine patterns, so an accurate etching process was developed to produce the ceramic tiles, and care was taken regarding the alignment of the parts during the assembly.
- The top metallization of the dies (aluminium) is not compatible with silver sintering, requiring a dedicated preparation process.
- The thin layer of silver cannot provide much compensation for any difference in height when several devices are to be assembled in the same sandwich, so the thickness must be well controlled.

The solutions developed to tackle these issues are presented in this article. In the first section, we present the

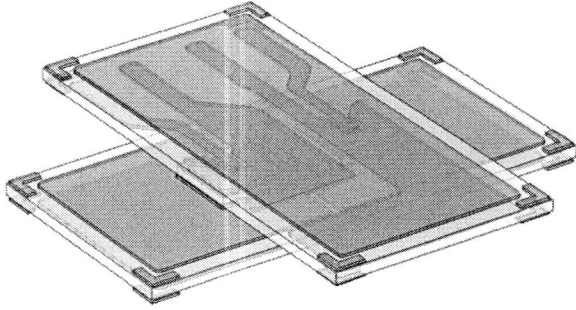


Figure 1: 3-D view of the "sandwich" structure, with two SiC JFET in half-bridge configuration. The ceramic tiles measure  $12.7 \times 25.4 \text{ mm}^2$  each.

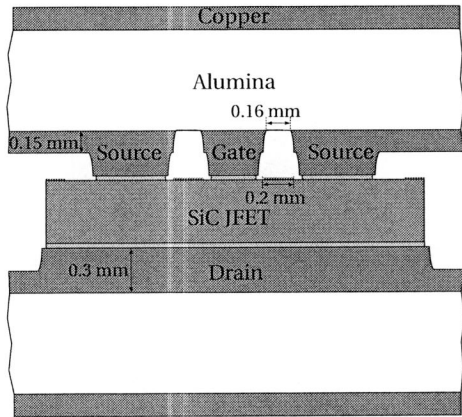


Figure 2: Up-to-scale cross section of the sandwich module around the SiC die (here a  $2.4 \times 2.4 \text{ mm}^2$  die) showing the relative thicknesses and spacing between the copper tracks. The alumina thickness is  $0.635 \text{ mm}$ , and that of the sintered-silver layer  $\approx 0,025 \text{ mm}$ .

sandwich structure. In the second section, the silver migration risk is assessed, and a solution is proposed to mitigate said risk. Finally, we present the manufacturing steps we used to produce working sandwich modules.

## 2 The "sandwich" structure

A 3D concept view of the sandwich module described in this paper is visible in figure 1. This module contains two SiC JFETs (SiCED, 1200 V), to form a half-bridge structure. The body diode of the JFETs is used so no external diodes are needed. Modules were made with two die sizes ( $2.4 \times 2.4 \text{ mm}^2$  and  $4 \times 4 \text{ mm}^2$  dies), requiring a dedicated set of DBC (ceramic) tiles for each die size, as they have different patterns.

A dual-step etching process comparable to that used in [8] is needed to produce the DBC tiles. This is depicted in figure 2: the inner copper layers have some protrusions

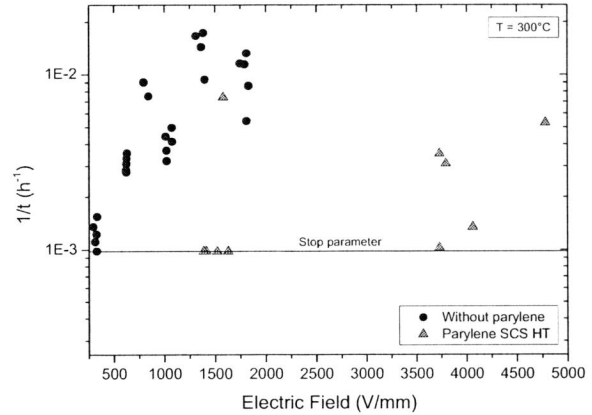


Figure 4: Time before a short circuit appears between the electrodes of a test sample as a result of silver migration, for an ambient temperature of  $300 \text{ }^\circ\text{C}$ , depending on the electric field applied, and for two sets of samples: unprotected (blue dots), and coated with a  $20 \mu\text{m}$  layer of parylene HT (yellow triangles).

where a contact is required with the die, and are thinner elsewhere. This keeps the copper conductors away from the edge protections of the die, which is required to maintain its blocking voltage capability.

Alumina-based DBC substrates were selected for this module based on cost considerations. Silicon Nitride, however, might prove to be a better option from a reliability point of view. No specific finish was applied on the copper layers, as silver sintering was found to work (albeit not optimally) on bare copper [9]. Here again, a better option might be a gold or silver-based finish (the exact composition will depend on the sintering paste).

## 3 Silver Migration

The silver migration phenomenon is described in [7]. Basically, it is related to the silver oxide becoming unstable at high temperature. To assess the extend of the issue, we manufactured special test samples, consisting of two silver electrodes stencil-printed on an alumina substrate. A photograph of some test samples is given in figures 3a and 3d, for an inter-electrodes gap of  $1 \text{ mm}$  (various gap values were investigated, from  $0.5$  to  $2 \text{ mm}$ , see [10]).

The test samples were placed in a forced-convection oven, with a voltage bias (up to  $1100 \text{ V}$ , using a Keithley Source and Measure Unit – SMU – 2410). Up to 10 samples were tested simultaneously, using a high-voltage switch system (Keithley 7001 with 7154 switch card). Periodically (every  $15 \text{ mn}$ ), the leakage current of each test sample was measured. When this current exceeded a given value ( $100 \mu\text{A}$ ), the corresponding test sample was disconnected and the test resumed with the remain-

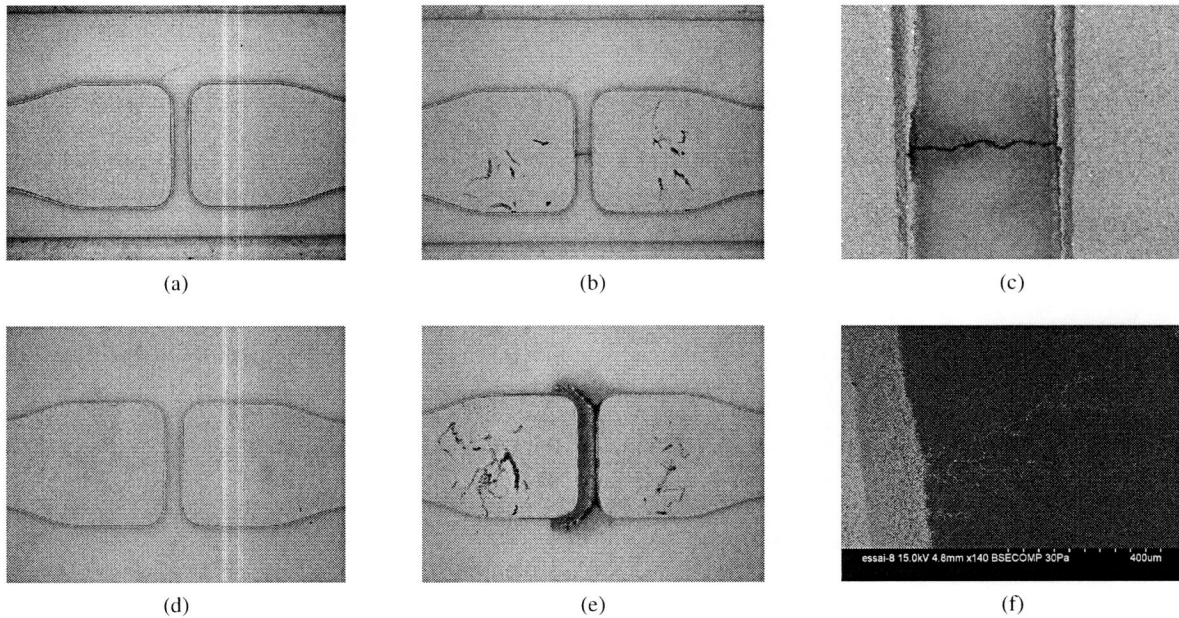


Figure 3: Pictures of some of the test samples, before the test (a) and (d), and after (b) and (e) respectively. An enlargement of (b) can be seen in (c), while an electron microscope view from another sample is visible in (f). It can be seen that the pattern and coverage of the silver deposit vary widely. All samples presented here have a 1 mm gap between electrodes

ing samples. The test was stopped once all test samples had failed, or after the test had run for 1000 h.

Tests were run for different gap sizes, different ambient temperature (from 250 to 300°C, different voltages (230 to 1100 V). In most cases, silver migration was observed in less than 1000 h. The migration patterns are quite different from one sample to the other, as can be seen in figures 3b (close-up in 3c) and 3e, all coming from the same test batch. A close-up view of a different sample, using a scanning electron microscope, shows the “dendritic” aspect of the silver filament.

The time before failure as a function of the electric field (voltage difference between the electrodes divided by the gap), at 300 °C ambient, is plotted with blue round dots in figure 4. As can be seen, the time before failure is fairly short, from less than 100 h ( $1\text{E-}2\text{ h}^{-1}$ ) up to 1000 h ( $1\text{E-}3\text{ h}^{-1}$ ), for electric field levels that can be experienced within a real power module (less than 1000 V/mm).

As described above, silver migration occurs in the presence of oxygen. To prevent migration to occur, an idea is therefore to coat the silver layers with an oxygen barrier. Parylene HT (SCS Coatings) was found in [11] to be a good oxygen barrier and to be able to withstand long-term operation at 300 °C. Furthermore, parylene has a vapour-phase deposition process that results in uniform and conformal coating, even on complicated shapes, as we will show later in this paper.

Test samples with a 20  $\mu\text{m}$  layer of parylene HT were

submitted to the same test conditions as the un-coated samples (300 °C ambient). The corresponding times-to-failure are plotted with yellow triangles in figure 4. A dramatic improvement can be observed with most samples matching the 1000 h parameter without failure. One test sample was found to fail at 134 h for a 1578 V/mm field, which is probably related to a manufacturing default.

As a consequence, Parylene HT can be considered as a suitable material to mitigate the risks associated with silver migration. It is important to note that the tests presented here constitute a worst-case configuration, with silver used as the electrode material. The electric field actually experienced by a sintered silver die attach should be lower.

## 4 Module Manufacturing

The various parts of the sandwich module are visible in figure 5, for both designs (one set for  $2.4\times 2.4\text{ mm}^2$  dies, another for  $4\times 4\text{ mm}^2$  dies): two DBC tiles, two JFET dies, and one small copper spacer. The DBC tile with the source and gate patterns (left) will be referred to as “source” substrate, and the other one as the “drain” substrate.

The manufacturing process can be summarized as follows:

- Etching of the DBC substrates: as the accuracy re-

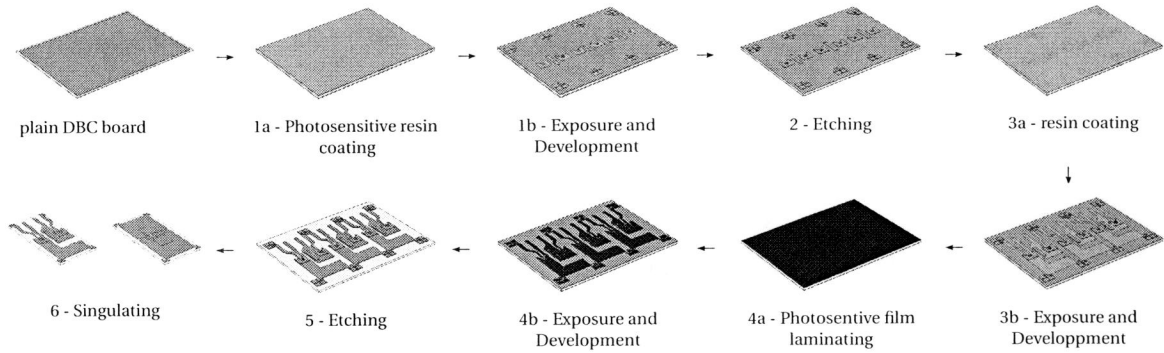


Figure 6: 2-level etching process to produce the DBC tiles.

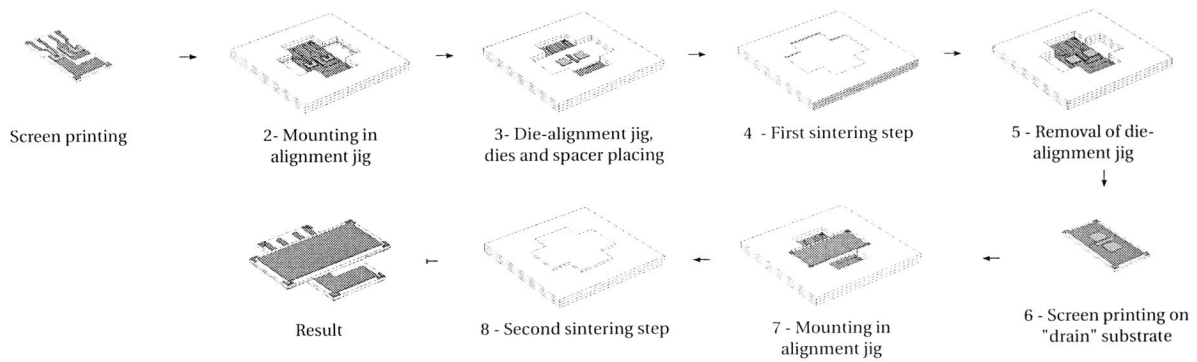


Figure 7: Assembly workflow, showing the ceramic jigs used to ensure a proper alignment of the parts. During the sintering steps, a piece of ceramic is placed over the parts for pressure distribution.

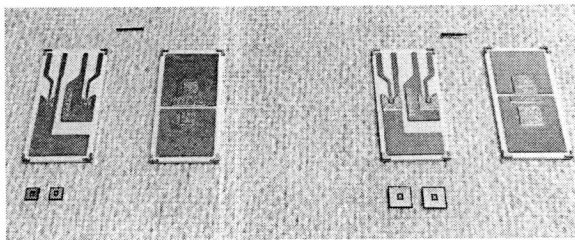


Figure 5: Two sets of parts (one for the  $2.4 \times 2.4 \text{ mm}^2$  JFET dies, one for the  $4 \times 4 \text{ mm}^2$  JFET dies) before assembly. A set comprises two ceramic tiles, two JFETs and one spacer.

quired (see figure 2) exceeds the design rules of the DBC manufacturers we know, a custom etching process was developed;

- Die topside metallization: the JFETs have an aluminium topside metal, suited to wirebonding but not to silver sintering. A plating step is therefore required to cover the aluminum with another metal (silver);
- Assembly, using silver sintering.

- Parylene HT coating of the module

#### 4.1 Etching of the DBC substrates

As described in section 2, a two-level etching process was required to create some copper protrusions to connect the dies. This process is described in figure 6: First, a photosensitive resin (MC dip coating, microchemicals) is applied on a plain DBC board by dip coating (6 mm/s withdrawal speed, 5 mn drying at  $100^\circ\text{C}$  in an oven). It is then exposed to UV light (Quintel Q-2001 CT mask aligner, 200 W mercury lamp, 90 s) through a mask and developed using ma-D 331 (micro resist technology). The exposed copper is etched half-way through using ferric chloride (6 minutes using a spray etcher).

After cleaning, the substrate goes through a second resin coating/exposure/development process. However, because of the features now present on the copper, the resin layer was found not to be uniform enough: the crests of the protrusions only have a very thin layer of resin, not sufficient to protect them from the ferric chloride. Therefore, an additional layer of photosensitive material (Dupont PM275 photosensitive dry film) is laminated on

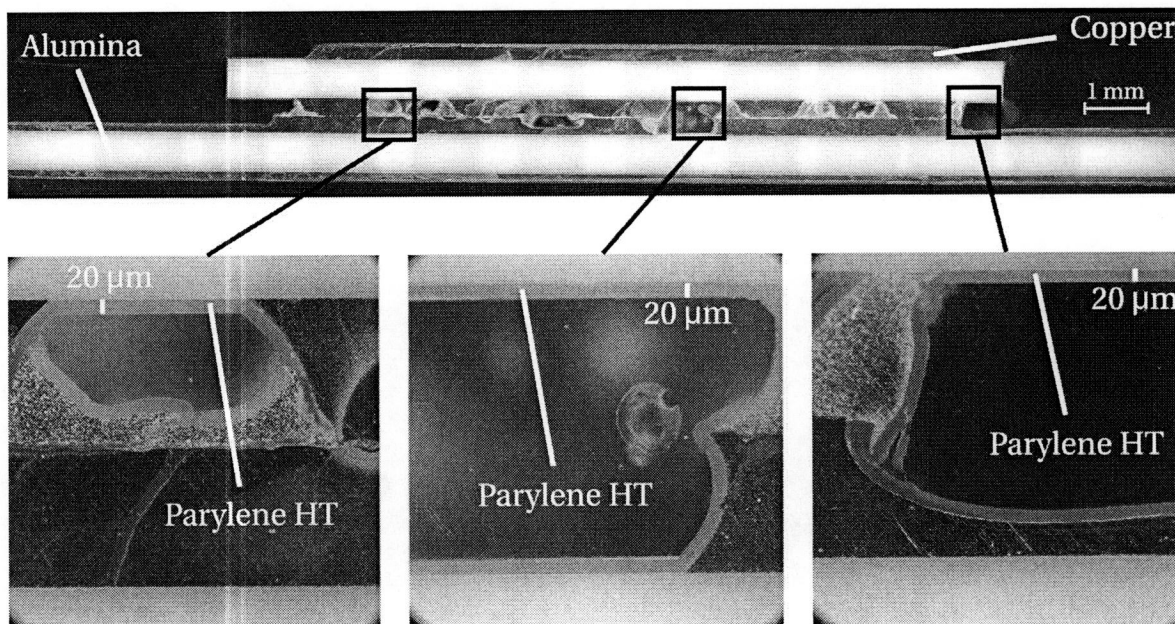


Figure 9: Cross section of a test assembly (no dies, poor control of copper etching and silver sintering) showing that the parylene HT coating is uniform over the entire sample, even in the most intricate cavities..

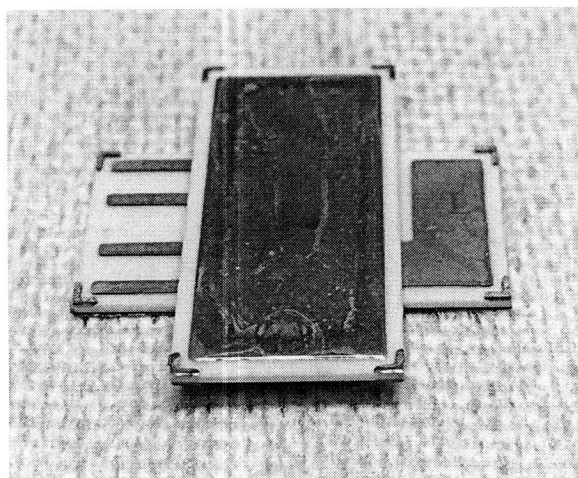


Figure 8: The module after assembly

top of the substrate (step 4a in figure 6), exposed and developed (using a 1% wt  $\text{Na}_2\text{CO}_3$  solution).

Finally, a second etching step is performed (9 mn), the photosensitive materials are removed in acetone, and the substrates are cleaned and singulated (using a disco DAD3220 wafer saw).

Overall, the copper features are found to be within  $50 \mu\text{m}$  of the desired dimensions, which is satisfying.

## 4.2 Plating of SiC dies

The JFET dies are mounted in a stainless-steel mask with openings matching their topside layout. The alignment is provided by pockets managed in the mask (DB Products). The mask and dies are then placed in an electron-gun evaporator (EVA300), for the deposition of Ti and Ag (200 nm).

## 4.3 Assembly

The assembly process is described in figure 7. The two sintering steps are performed using Heraeus LTS-117O2P2 silver paste. First, a  $50 \mu\text{m}$ -thick layer of silver paste is stencil-printed on the substrate. Then a short 5-minute drying at  $85^\circ\text{C}$  is performed to prevent the silver paste to flow while keeping some tackiness. The parts to join are put in contact, using some alignment jigs (laser cut alumina), and placed on the heating platen of the sintering press. A 30 mn,  $85^\circ\text{C}$  drying step is then performed, followed by a  $70^\circ\text{C}/\text{mn}$  ramp and a 30 mn,  $240^\circ\text{C}$  sintering step under a pressure of 2 MPa.

A picture of the resulting module is visible in figure 8. No cleaning was attempted after assembly, which explains the clearly visible oxidation marks on the copper. A low power electrical characterization showed that the module was functional (no short or open circuit) and that no change in performance of the devices could be observed.

#### 4.4 Parylene coating

Because of time constraints, parylene HT coating was attempted on a non-functional, preliminary assembly with no dies. A cross section of this test vehicle is visible in figure 9. It shows that parylene forms a very uniform layer all over the module, even in the most intricate parts. Along with the high temperature results from section 3, this proves that parylene is a very attractive solution for the encapsulation of high temperature power modules.

### 5 Conclusion

A “sandwich” structure comprising only high-temperature suited elements and materials has been presented. It uses silver sintering as a bonding material, and parylene HT to prevent silver migration. The complete manufacturing process, which offers a resolution compatible with the fine layout of the SiC dies has been described in details. Short term developments consist in high voltage (540 V) tests on parylene-HT-coated functional samples over the whole temperature range.

### Acknowledgement

The authors would like to thank EURIPIDES and CATRENE for their financial support of this work under the grant name “THOR”, and SCS for the parylene coating of our samples.

### References

- [1] C. Raynaud, D. Tournier, H. Morel, and D. Planson, “Comparison of high voltage and high temperature performances of wide bandgap semiconductors for vertical power devices,” *Diamond and Related Materials*, vol. 19, no. 1, pp. 1 – 6, 2010. [Online]. Available: <http://www.sciencedirect.com/science/article/B6T WV-4XCJ4M2-1/2/76c76271c9345b177d4fc29077179d2a>
- [2] J. Millán, P. Godignon, X. Perpiñà, A. Pérez-Tomás, and J. Rebollo, “A Survey of Wide Bandgap Power Semiconductor Devices,” *IEEE transactions on Power Electronics*, vol. 29, no. 5, pp. 2155–2163, may 2014.
- [3] C. Buttay, R. Ouaida, H. Morel, D. Bergogne, C. Raynaud, and F. Morel, “Thermal Stability of Silicon Carbide Power JFETs,” *IEEE transactions on Electron Devices*, vol. 60, no. 12, pp. 4191–4198, dec 2013.
- [4] J. Schulz-Harder, “Review on Highly Integrated Solutions for Power Electronic Devices,” in *Proceedings of the Conference on Integrated Power electronics Systems (CIPS)*, Nüremberg, mar 2008, p. 7 p. [Online]. Available: <http://www.electrovac.com/sprache2/n221666/n.html>
- [5] Z. Liang, P. Ning, F. Wang, and L. Marlino, “Reducing Parasitic Electrical Parameters with a Planar Interconnection Packaging Structure,” in *Integrated Power Electronics Systems (CIPS), 2012 7th International Conference on*. IEEE, 2012, pp. 1–6.
- [6] V. Manikam and K. Y. Cheong, “Die Attach Materials for High Temperature Applications: A Review,” *Components, Packaging and Manufacturing Technology, IEEE Transactions on*, vol. 1, no. 4, pp. 457–478, april 2011.
- [7] Y. Mei, D. Ibitayo, X. Chen, S. Luo, and G.-Q. Lu, “Migration of Sintered Nanosilver Die-attach Material on Alumina Substrate at High Temperatures,” in *Proceedings of the IMAPS International Conference and Exhibition on High Temperature Electronics (HiTEC 2010)*. albuquerque, NM: IMAPS, may 2010, pp. 26–31.
- [8] C. Buttay, J. Rashid, C. Johnson, F. Udrea, G. Amaratunga, P. Ireland, and R. Malhan, “Compact Inverter Designed for High-Temperature Operation,” in *Proc. IEEE Power Electronics Specialists Conference PESC 2007*, 2007, pp. 2241–2247.
- [9] S. Hascoët, C. Buttay, D. Planson, R. Chiriac, and A. Masson, “Pressureless Silver Sintering Die-Attach for SiC Power Devices,” *Materials Science Forum*, vol. 740, pp. 851–854, 2012.
- [10] R. Riva, C. Buttay, B. Allard, and P. Bevilacqua, “Migration issues in sintered-silver die attaches operating at high temperature,” *Microelectronics Reliability*, vol. 53, pp. 1592–1506, 2013. [Online]. Available: <http://dx.doi.org/10.1016/j.microrel.2013.07.103>
- [11] M. L. Locatelli, S. Diahm, Z. Valdez-Nava, M. Bechara, and R. Khazaka, “Suitable Characterization Methods and Insulating Materials for Devices Operating above 200 °C,” *Advanced Materials Research*, vol. 324, pp. 229–232, aug 2011. [Online]. Available: <http://www.scientific.net/AMR.324.229>